Observational Cosmology

Lectures on the topic:
Cosmology with galaxy clusters

(K. Basu)

Course website:
http://www.astro.uni-bonn.de/~kbasu/ObsCosmo
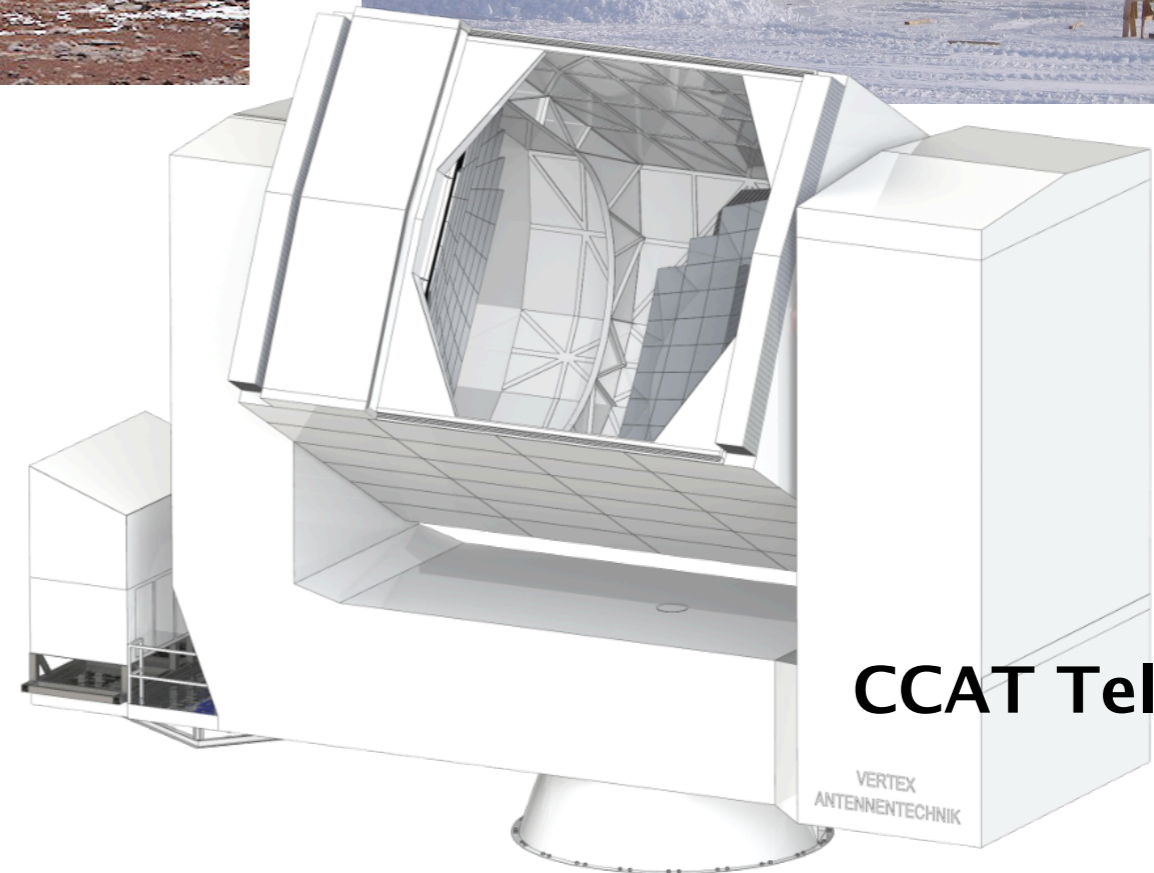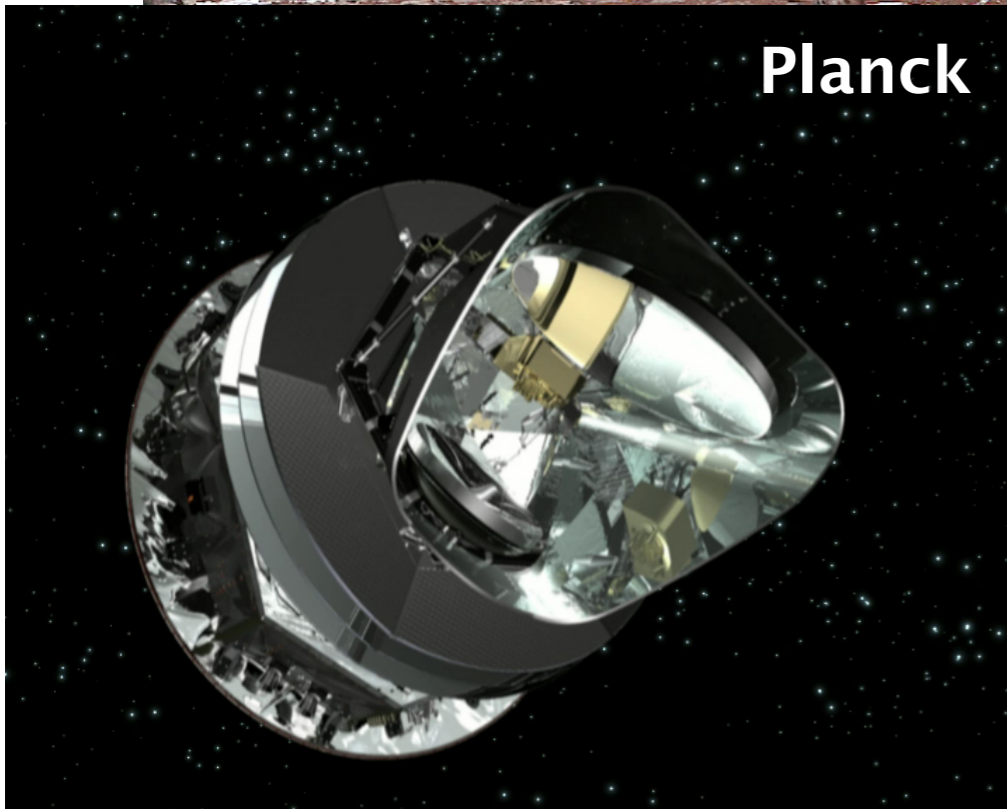
SZ Experiments

SZ cluster surveys

Atacama Cosmology Telescope (ACT)

South PoleTelescope (SPT)

Planck

CCAT Telescope

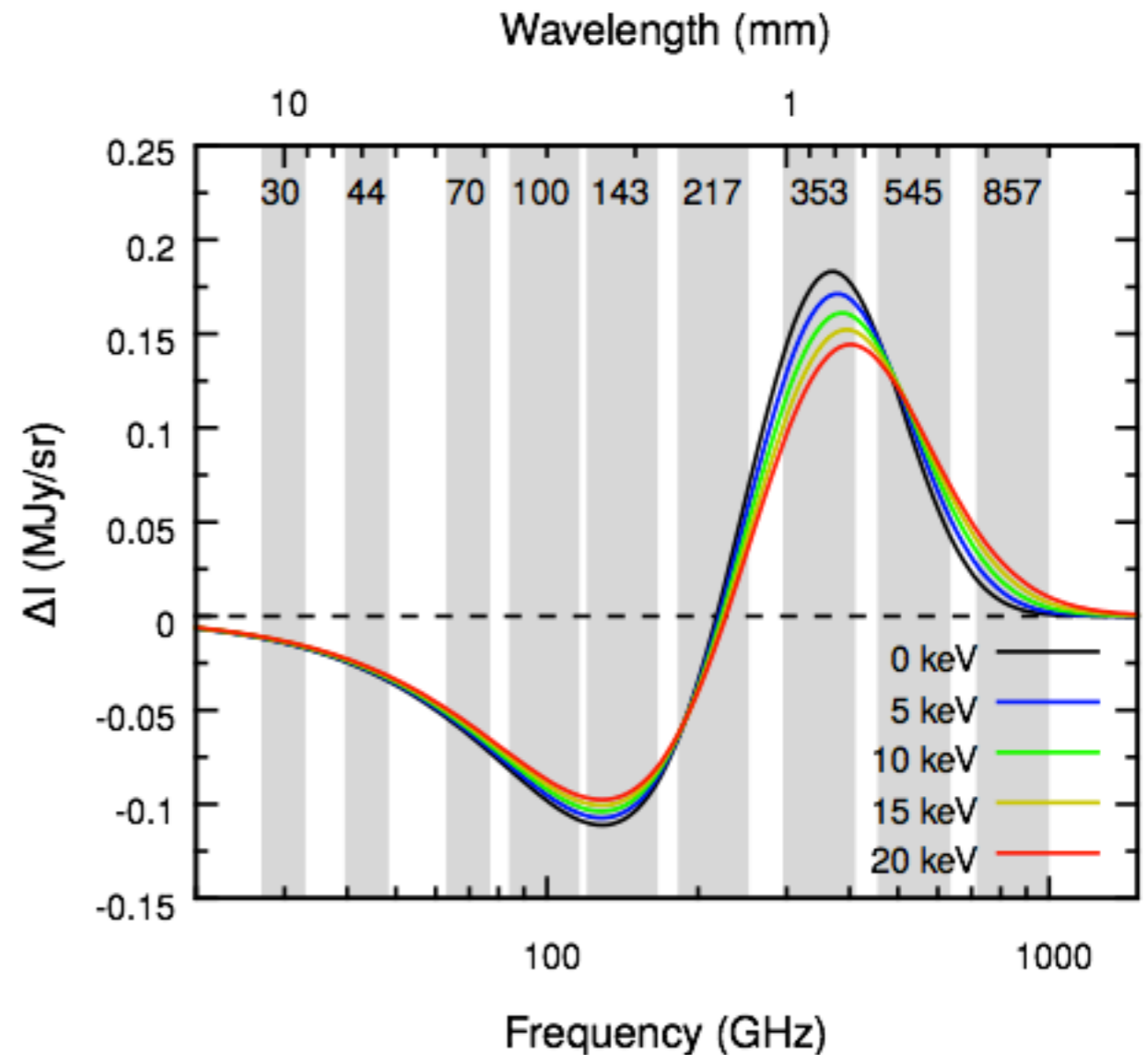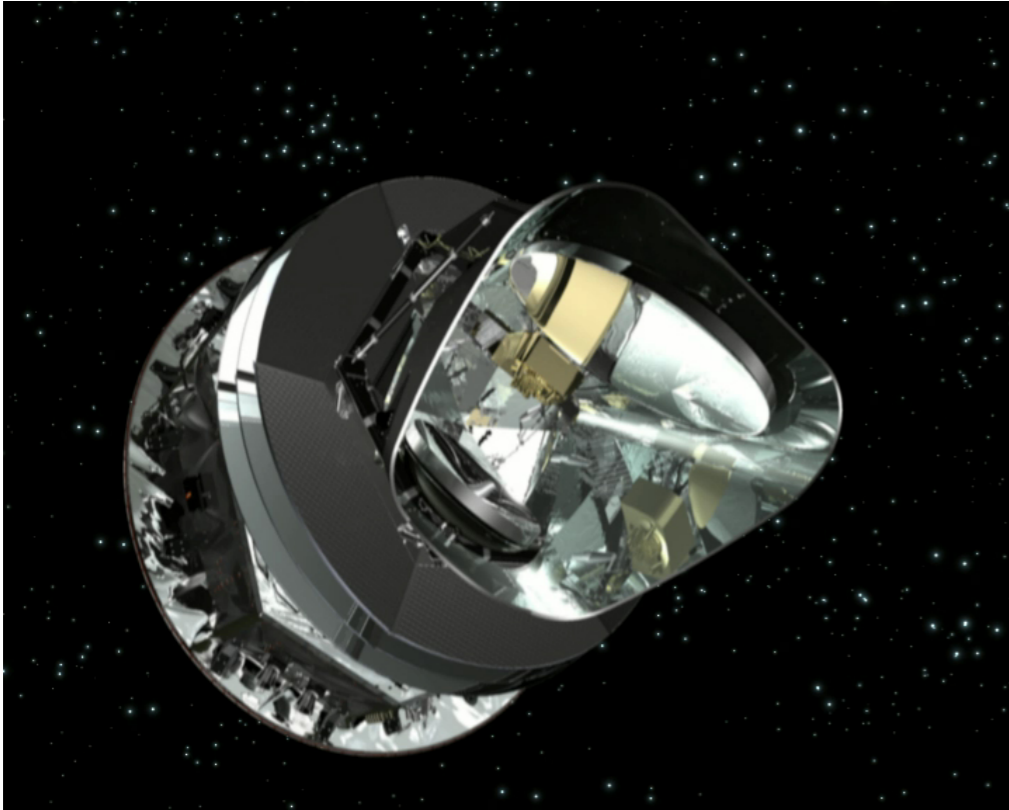# SPT–SZ clusters

Bleem et al. (2015)
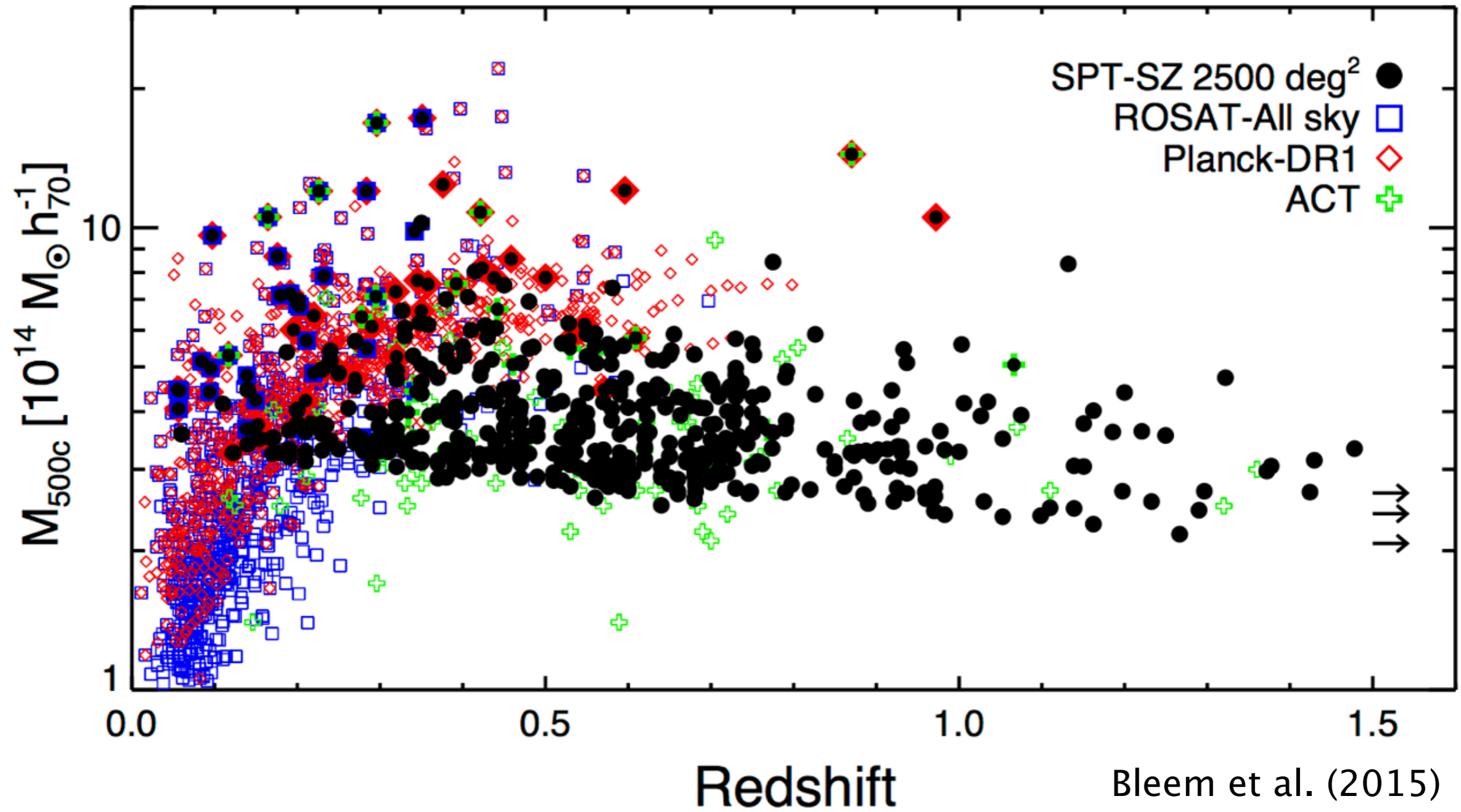
SPT–3G and the future
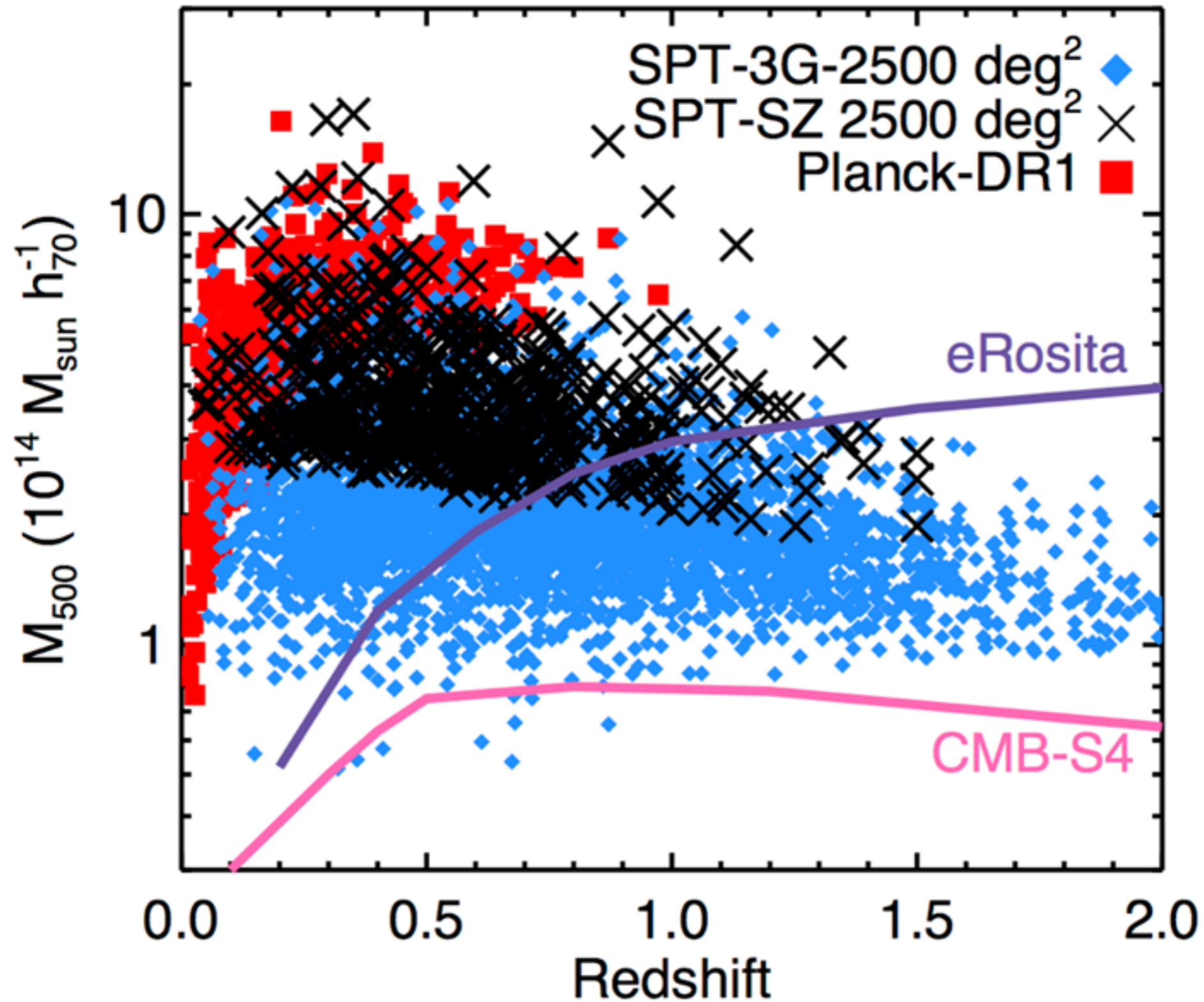
Planck SZ measurements

The wide frequency coverage of Planck (30 GHz – 850 GHz) enables excellent separation of the cosmological signal (CMB) from other Galactic and extragalactic foregrounds. One such "foreground" is the Comptonization distortion (SZ effect) of the CMB. Planck made the first all-sky map of the SZ effect.

y-maps from Planck data

Master's thesis of Jens Erler

(Planck collaboration 2015)
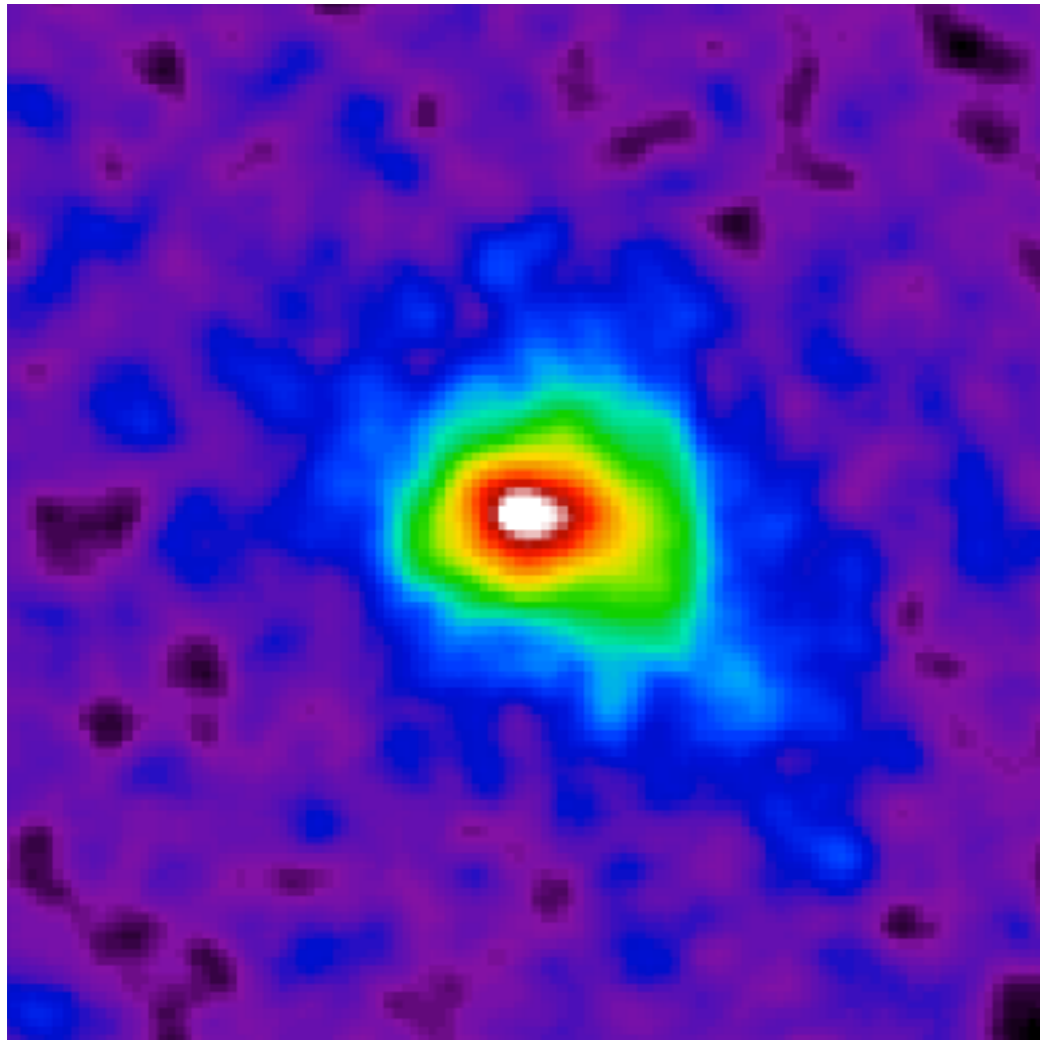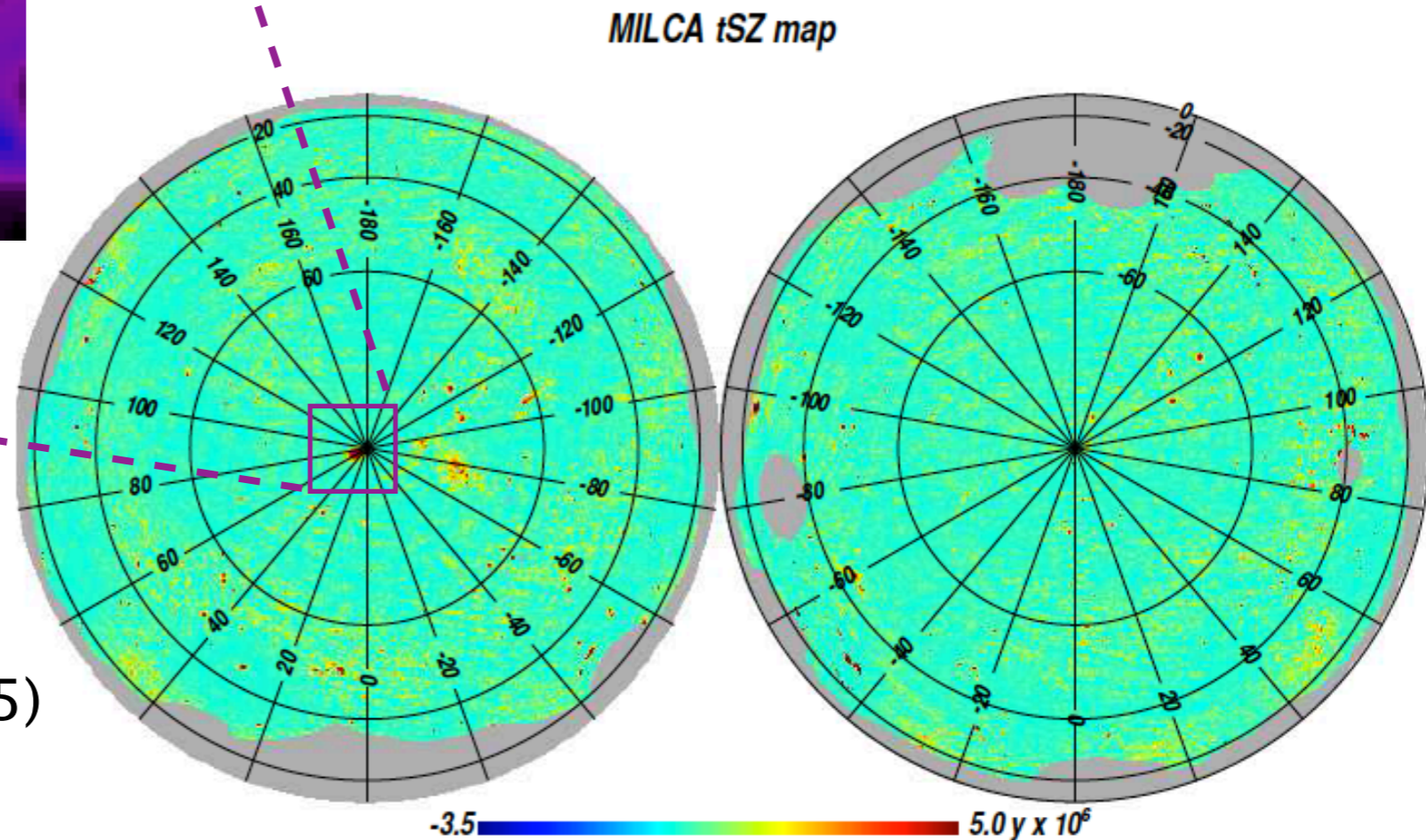
The Comptonization parameter maps (y-maps) are made using a method called Internal Linear Combination (ILC), which takes advantage of the very specific frequency spectrum of the thermal SZ effect to separate it from other astrophysical components.
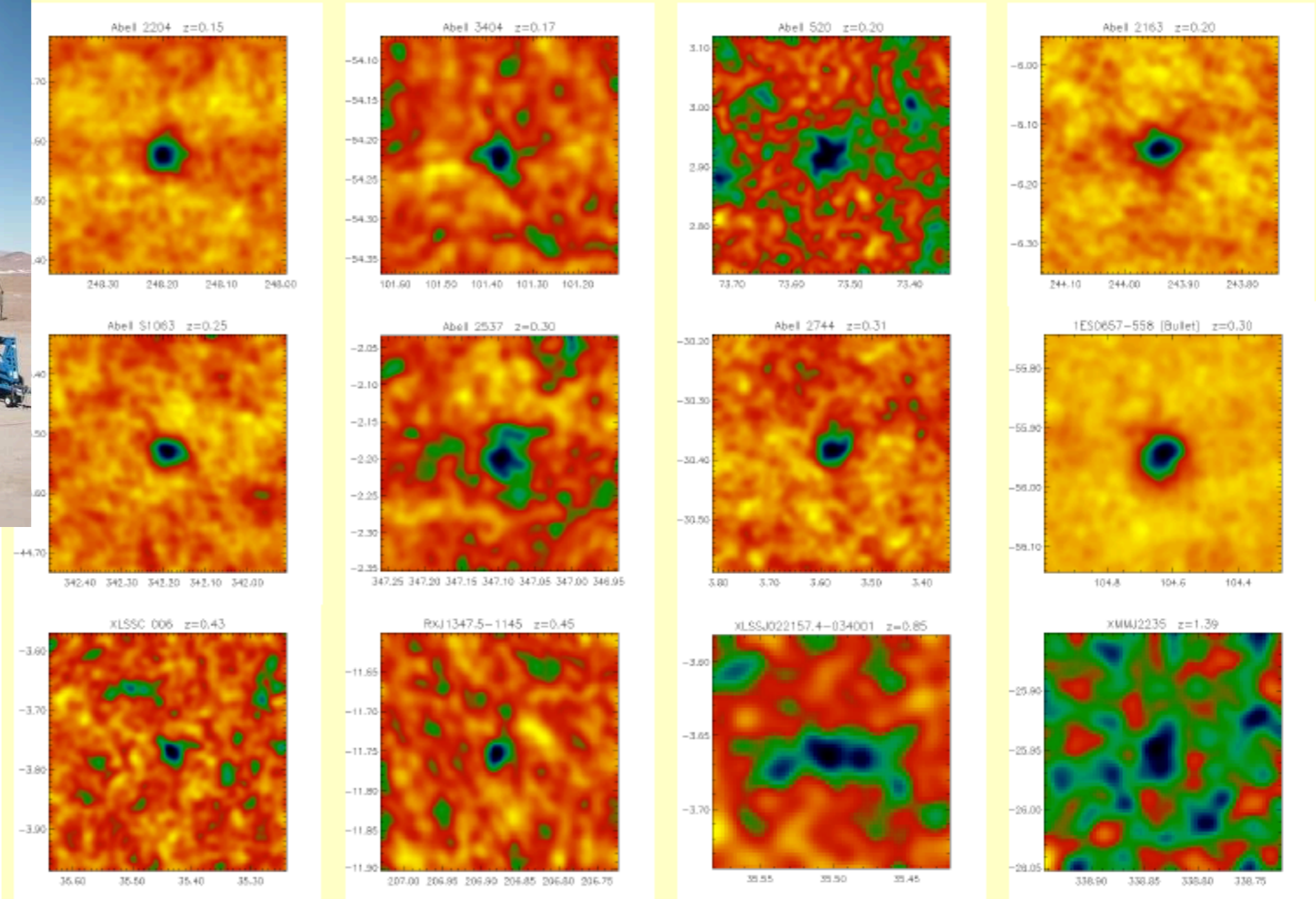
MILCA tSZ map

-3.5 $5.0\ y \times 10^6$

APEX telescope & its SZ detections

The APEX–SZ bolometer was operational in Chile between 2007–2010 and observed about 40 clusters in SZ effect at 150 GHz.

Halverson et al. 2009
Nord et al. 2009
Reichert et al. 2009
Basu et al. 2010
Bender et al. 2016
Nagarajan et al. (submitted)

The CCAT-prime telescope

CCAT-prime is a submillimeter telescope under construction at 5600 m altitude in Chile. It will start operating in 2021 and will provide the same frequency coverage as Planck and roughly 10 times better sensitivity.

Bonn and Cologne are partners in this project, along with Cornell, MPA, LMU, and some Canadian universities.
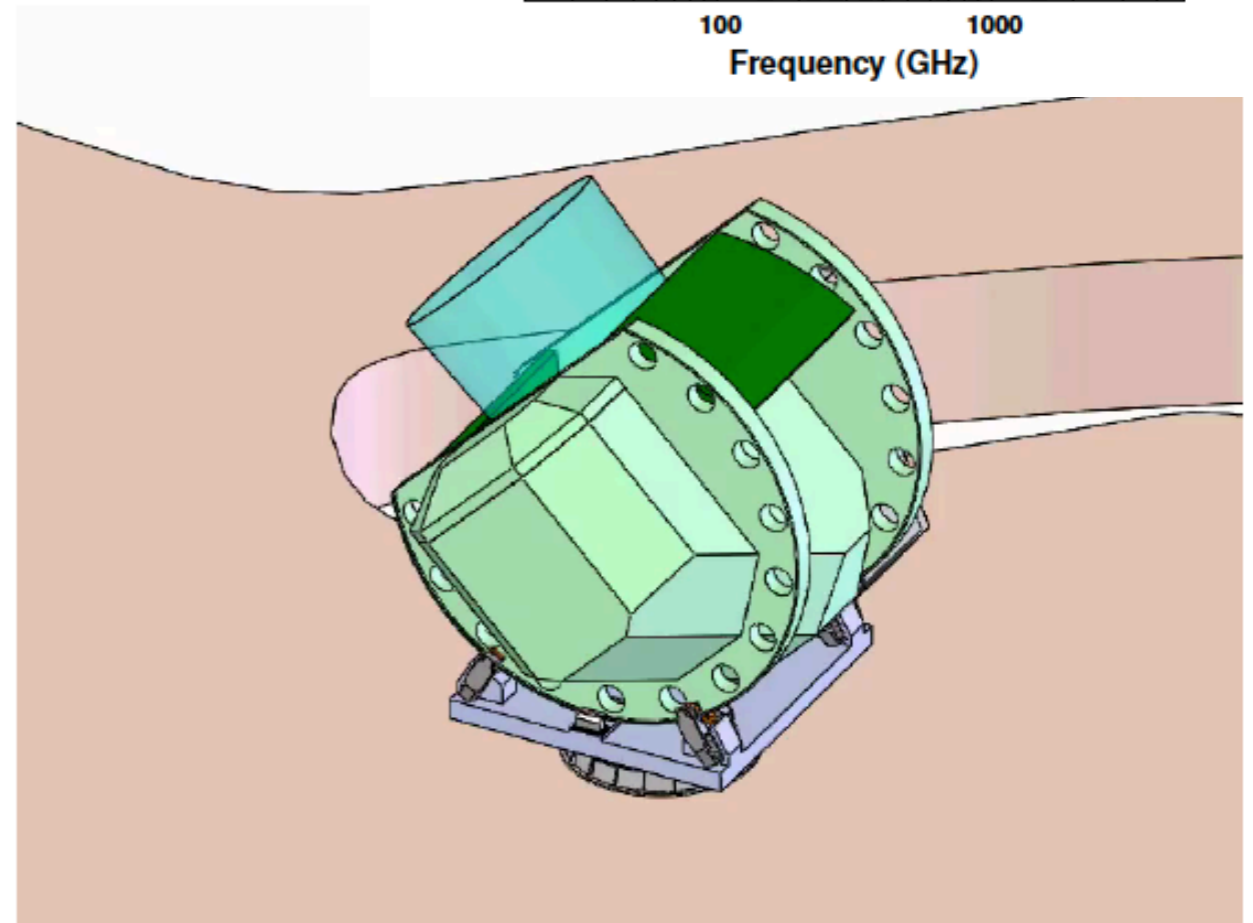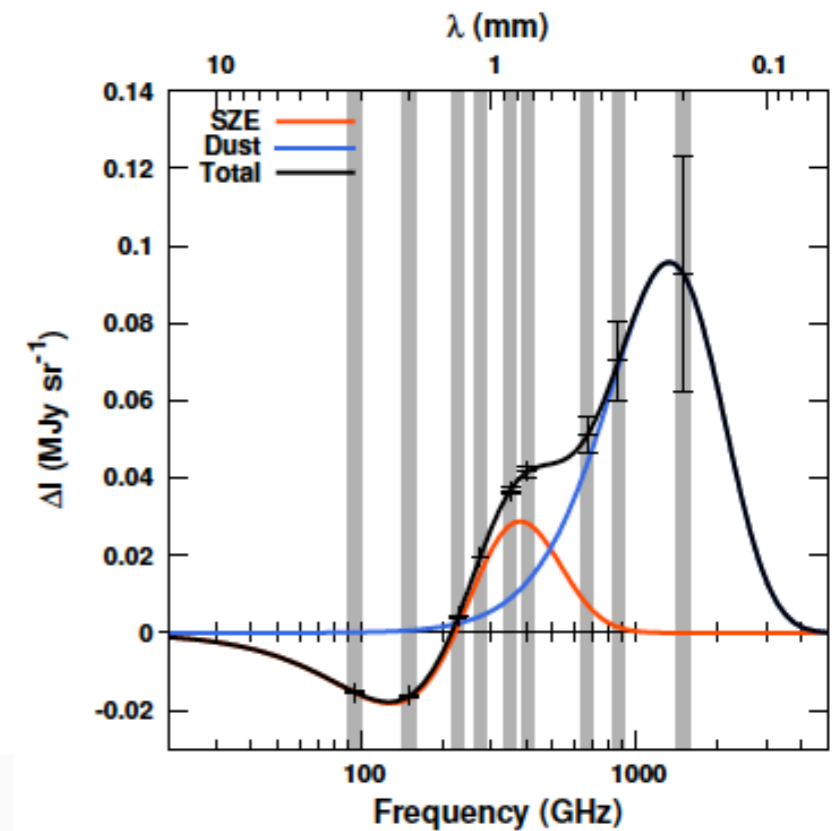
Thermal SZ power spectrum

SZ power spectrum

Lightly filtered map - 90 GHz

225 deg²

filtered map

point sources (in emission)

90 GHz   225 deg²

Primary CMB anisotropy

150 GHz

(grayscale +/- 100uK_CMB)

90 GHz   220 GHz
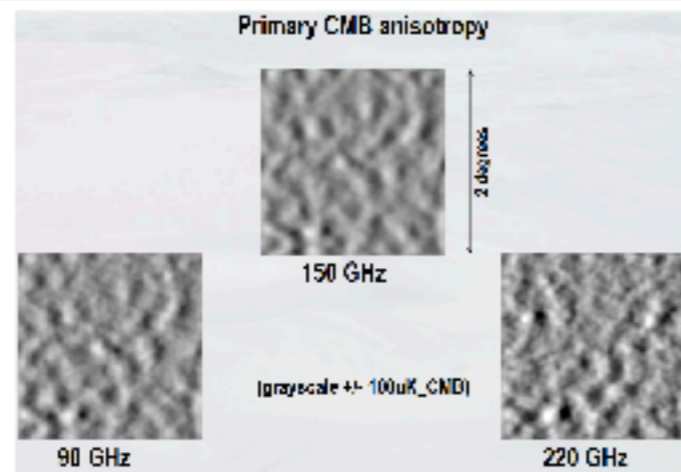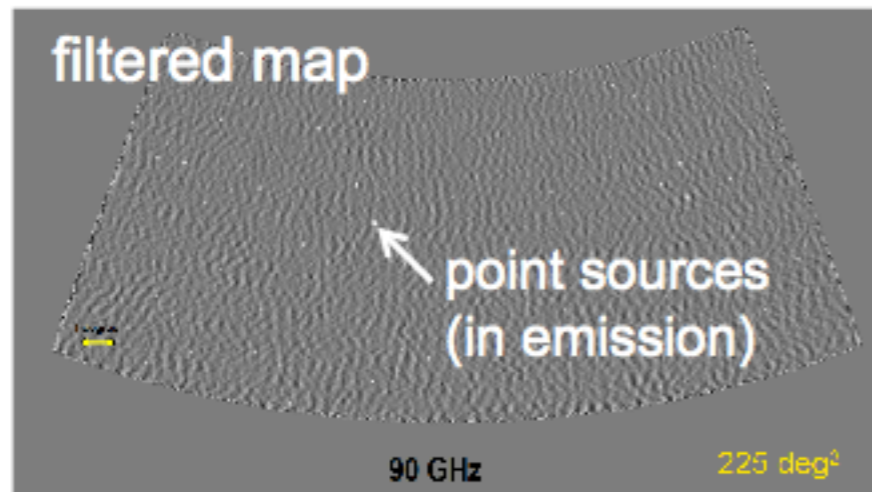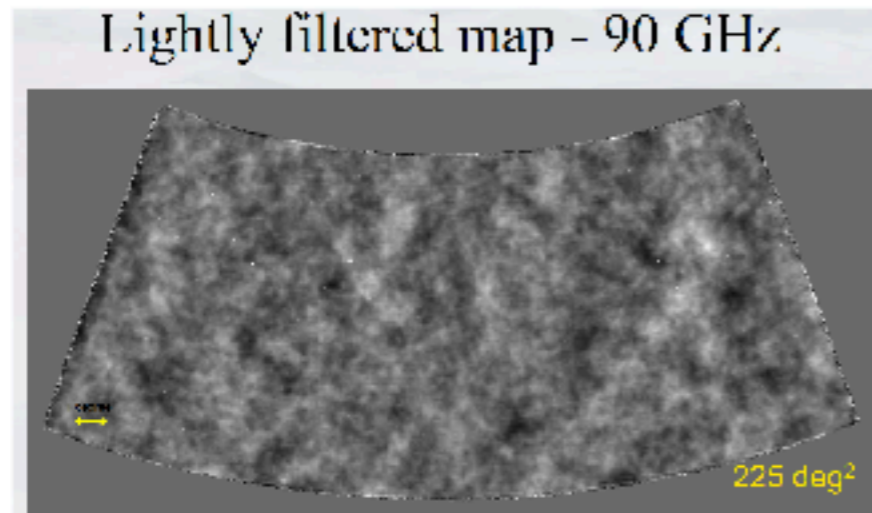
**Cluster Finding in
Real SPT Observations**

Raw   Filtered

40'

-12 σ

galaxy cluster
(decrement)

-8 σ
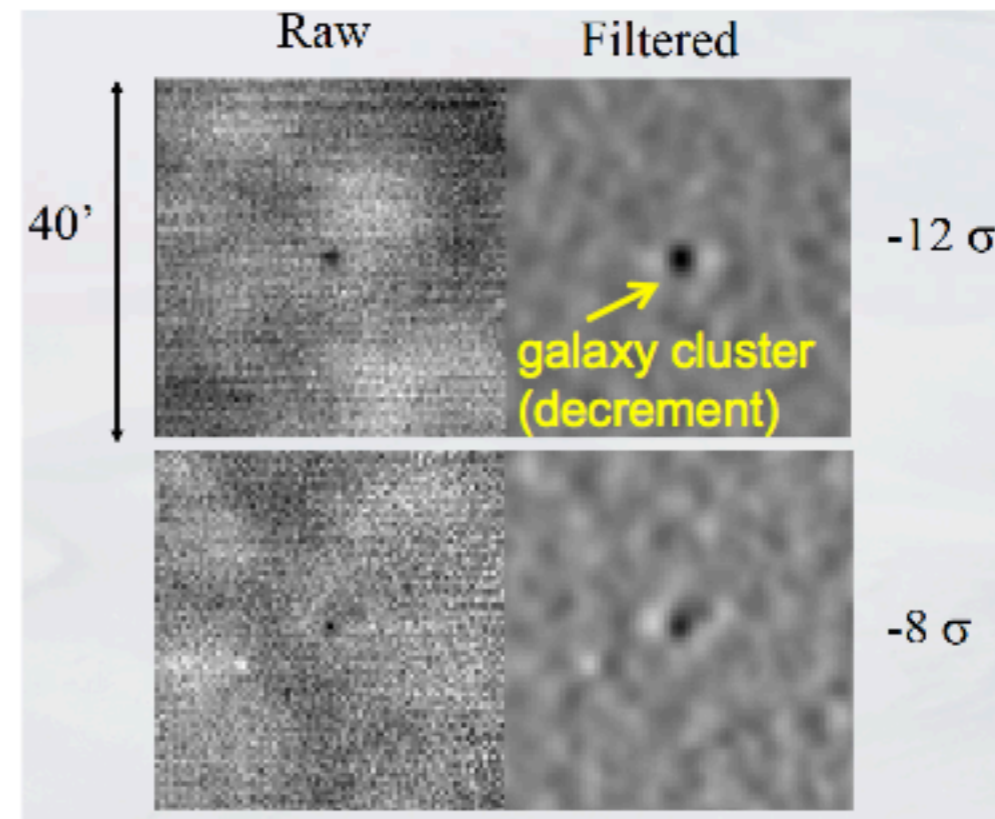
Source: http://member.ipmu.jp/clj2010//program_files/Talks/holzapfel.pdf

SZ power spectrum

150Ghz

Fourier Transform

simulated tsz map

10deg

$(D_l = l \, (l+1) \, c_l \, / \, 2\pi)$

16

Simulations from Shaw et al. (09); Sehgal et al. (10)
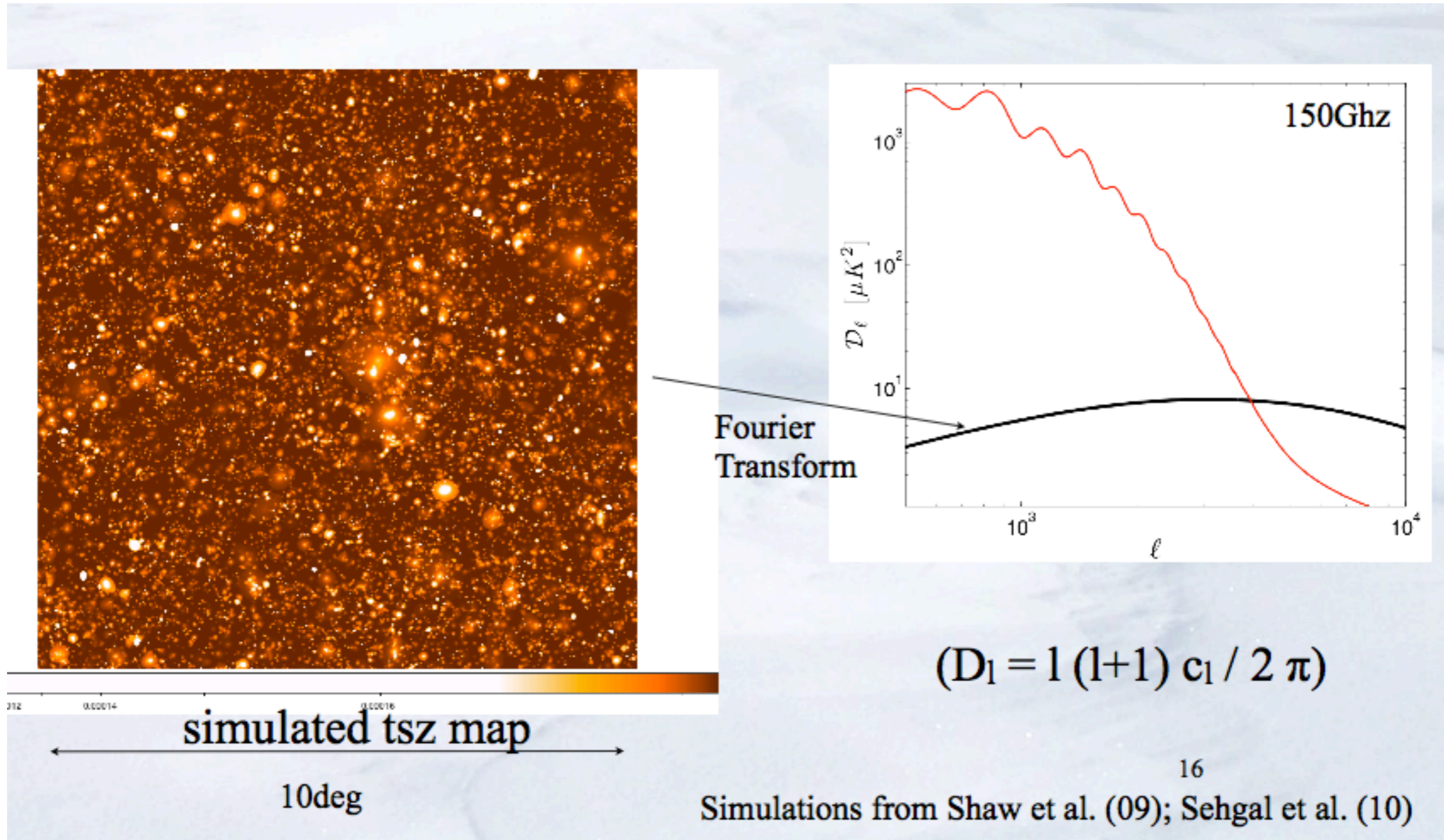
SZ power spectrum

Komatsu & Kitayama (1999)

SZ power spectrum

Cosmology | Astrophysics

$$C_l = f_\nu^2(x) \int_0^{z_{\max}} dz \frac{dV}{dz} \int_{M_{\min}}^{M_{\max}} dM \frac{dn(M,z)}{dM} |\tilde{y}_l(M,z)|^2$$

Spectral function

Co-moving volume

Halo mass function

Compton *y*-parameter

$$\tilde{y}_l = \frac{4\pi r_c'}{l_c^2} \int dx' \, x'^2 y_{3D}(x') \frac{\sin(lx'/l_c)}{lx'/l_c} \quad \longrightarrow \quad y_{3D}(x) \equiv \frac{\sigma_T}{m_e c^2} P_e(x)$$

SZ power cosmology dependence

Amplitude of SZ power spectrum has sensitive dependence on matter power spectrum normalization

$$C_\ell \propto \sigma_8^{7-9} (\Omega_b h)^2$$
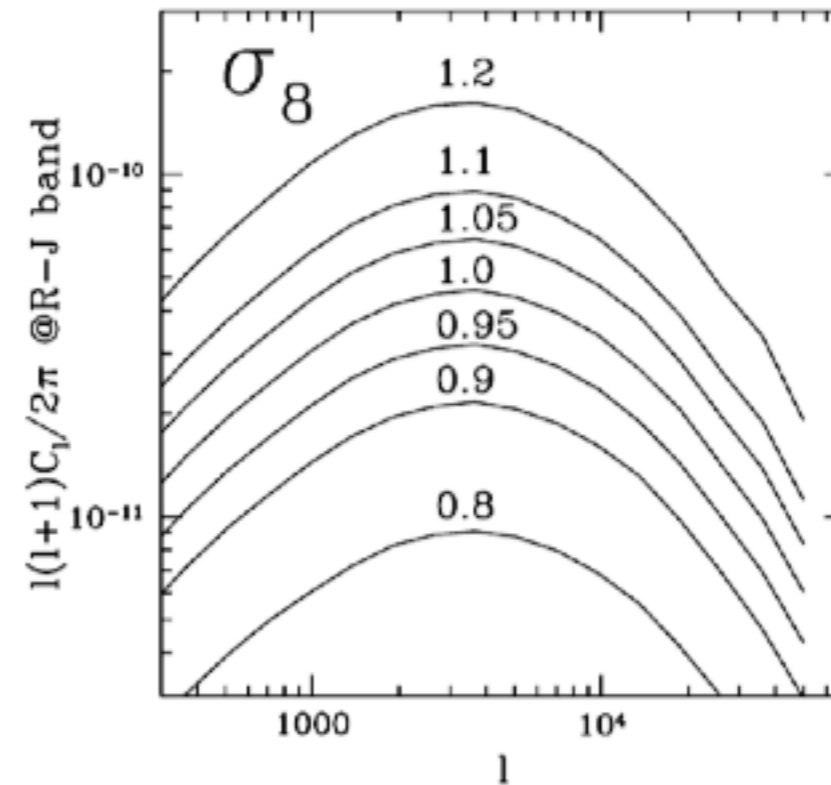
Figure 2. Dependence of the SZ angular power spectrum on σ_8. From top to bottom, the lines indicate $\sigma_8 = 1.2, 1.1, 1.05, 1.0, 0.95, 0.9,$ and 0.8, as shown in the figure.

Komatsu & Seljak
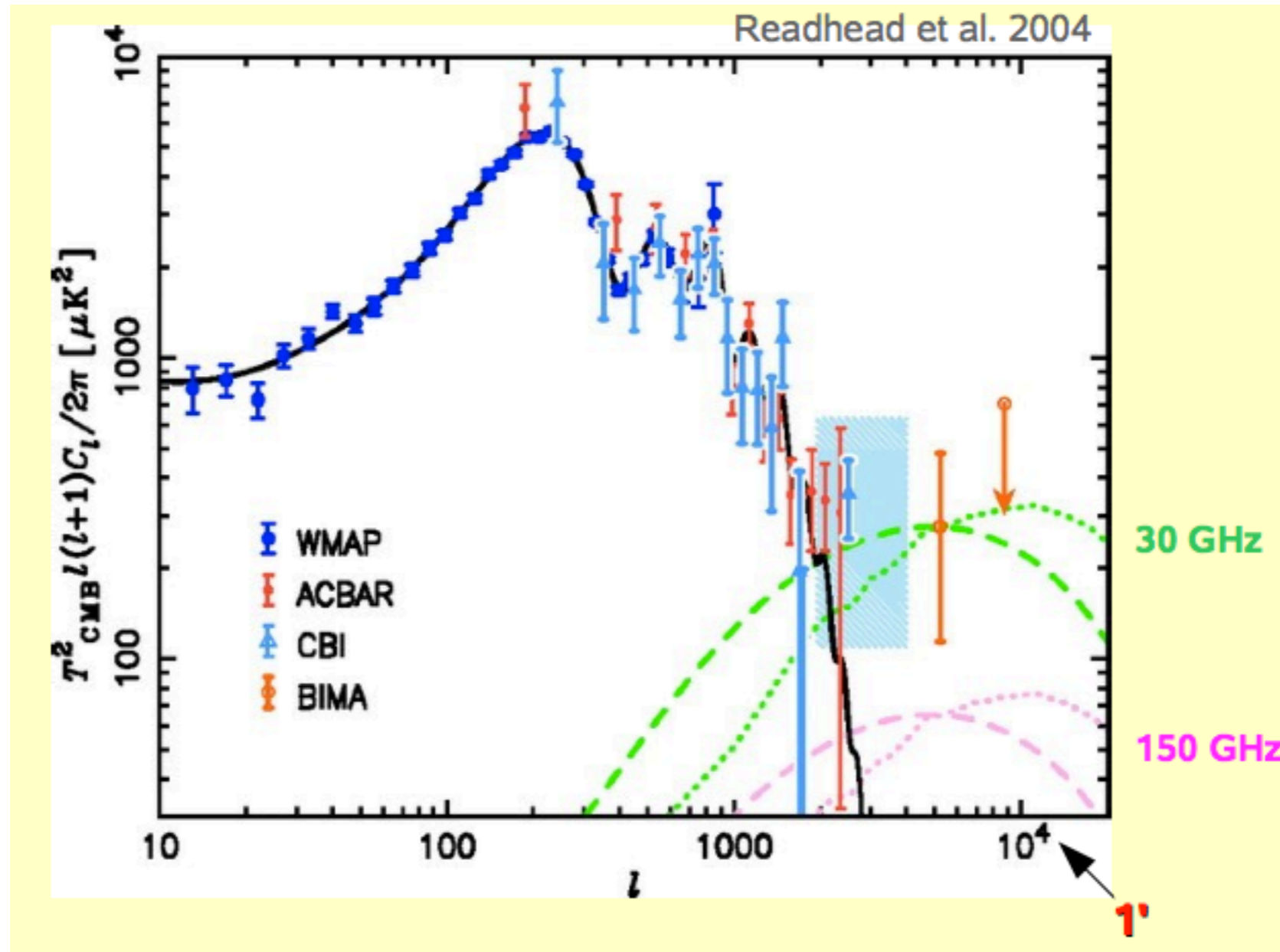
SZ power measurement

SZ power measurement

Lueker et al. (2009)

$$C_\ell \propto \sigma_8^{7-9}(\Omega_b h)^2$$

SZ power measurement
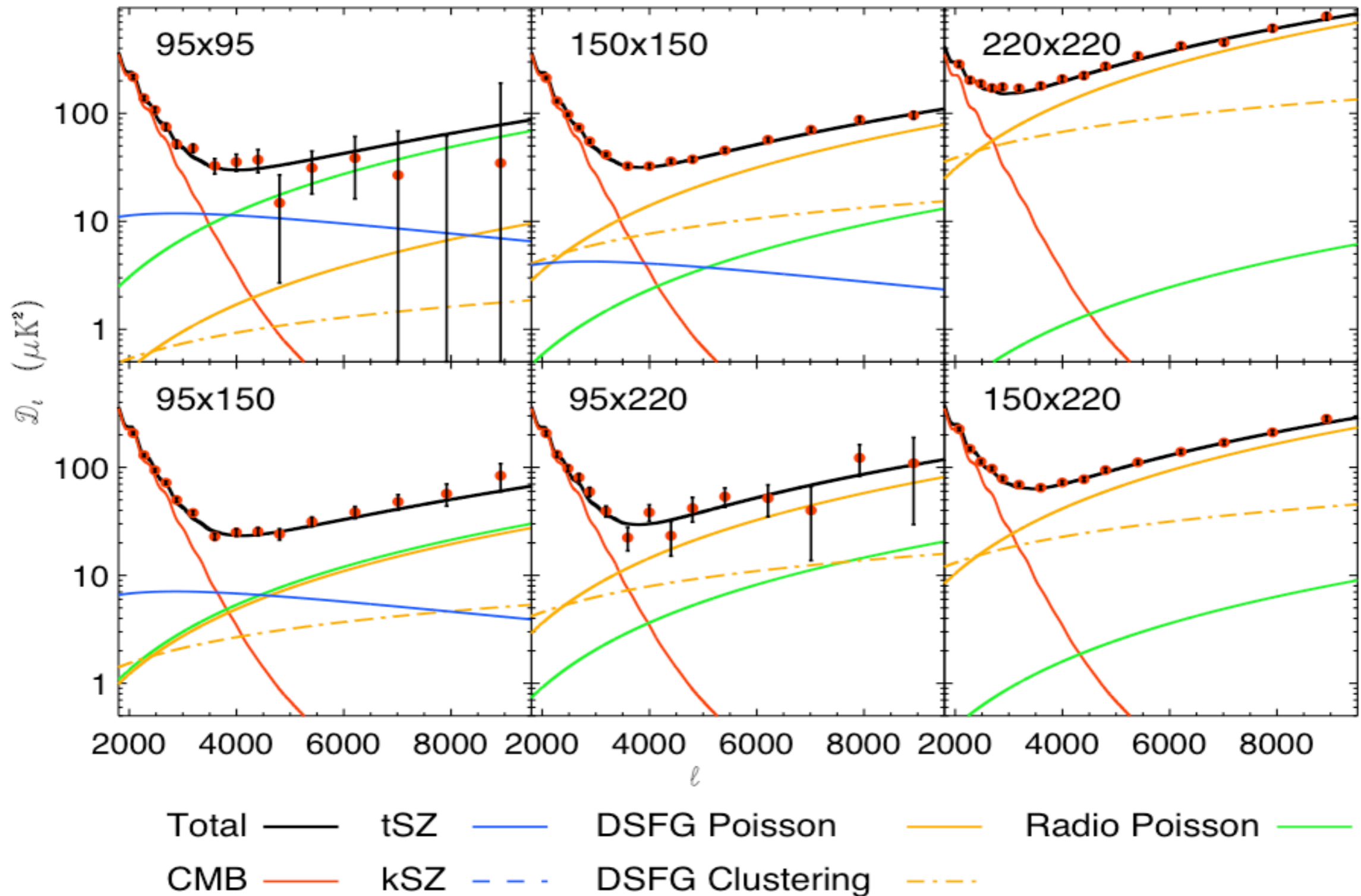
tSZ power spectrum "discrepancy"
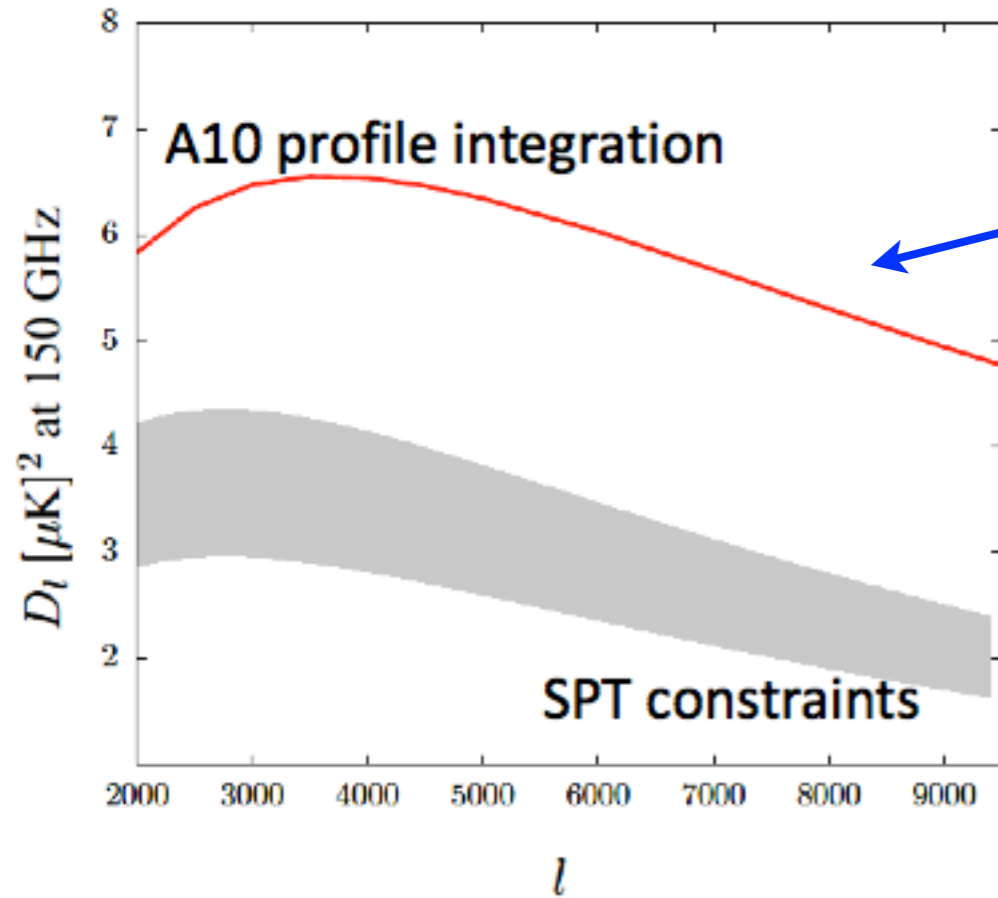
The discrepancy is most likely due to our wrong modeling of cluster astrophysics
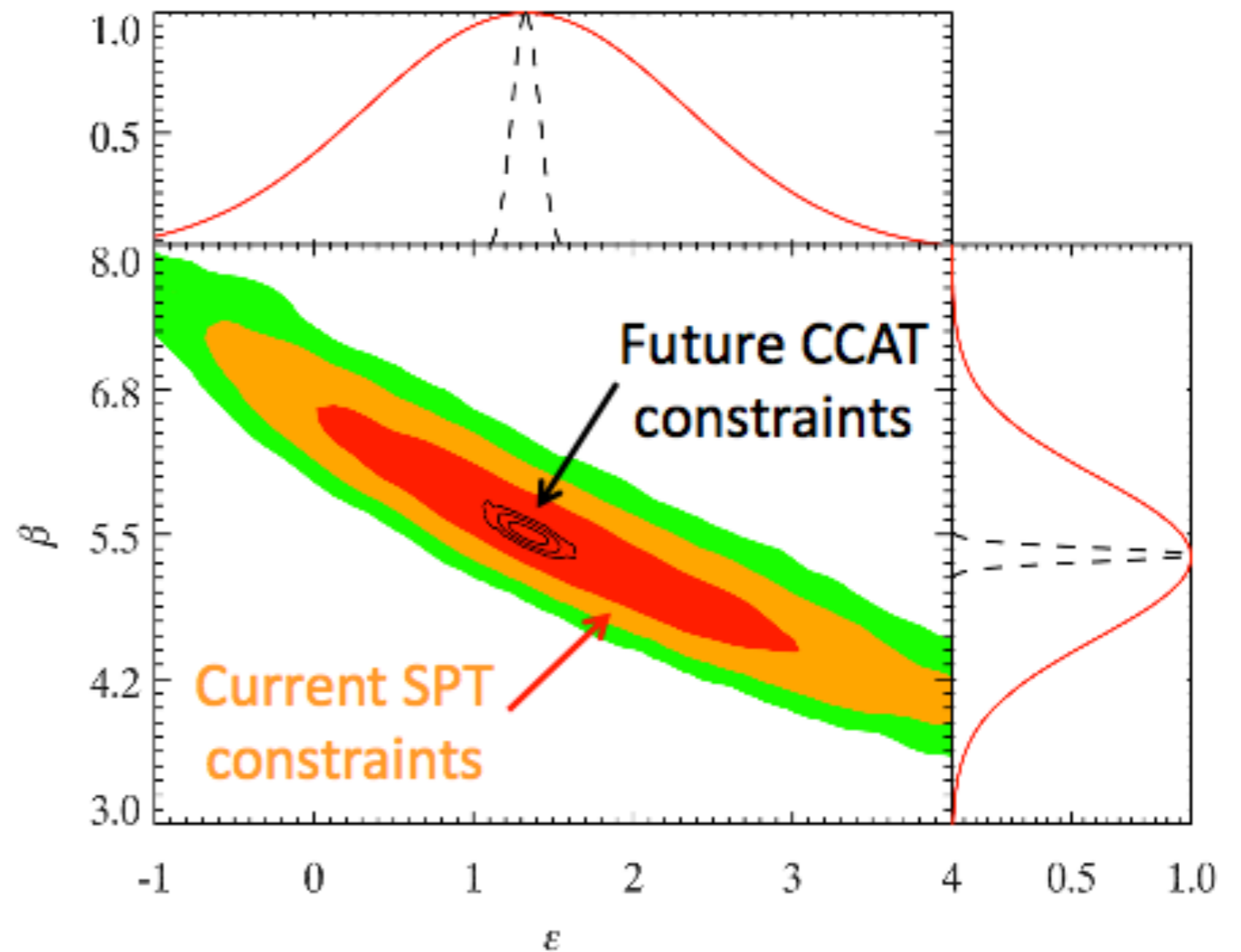
Ramos–Ceja, Basu, Pacaud (2014)

tSZ power "tension"
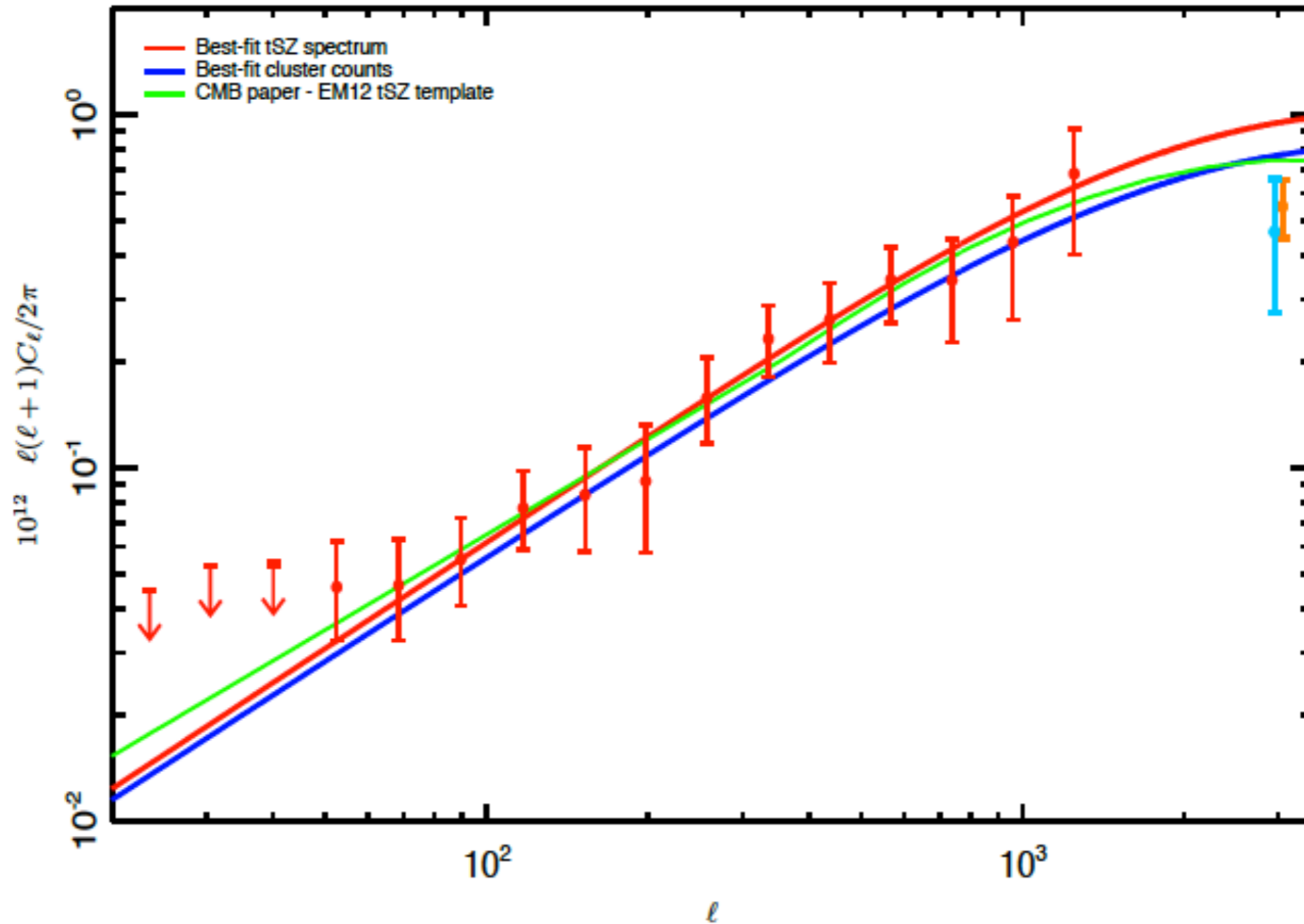
(Planck collaboration 2013)

tSZ power "skewness"

ACT data, Wilson et al. 2012
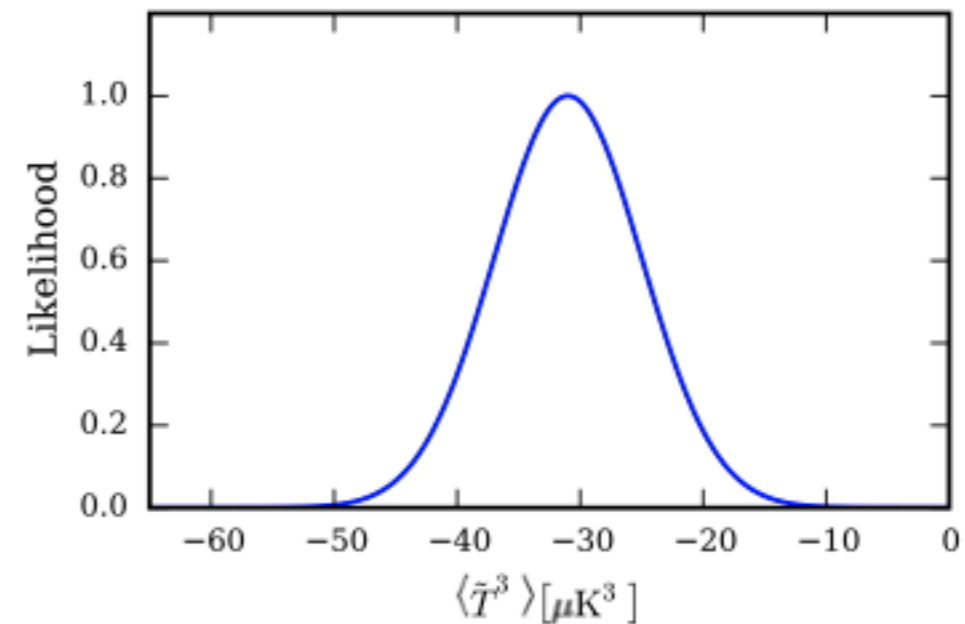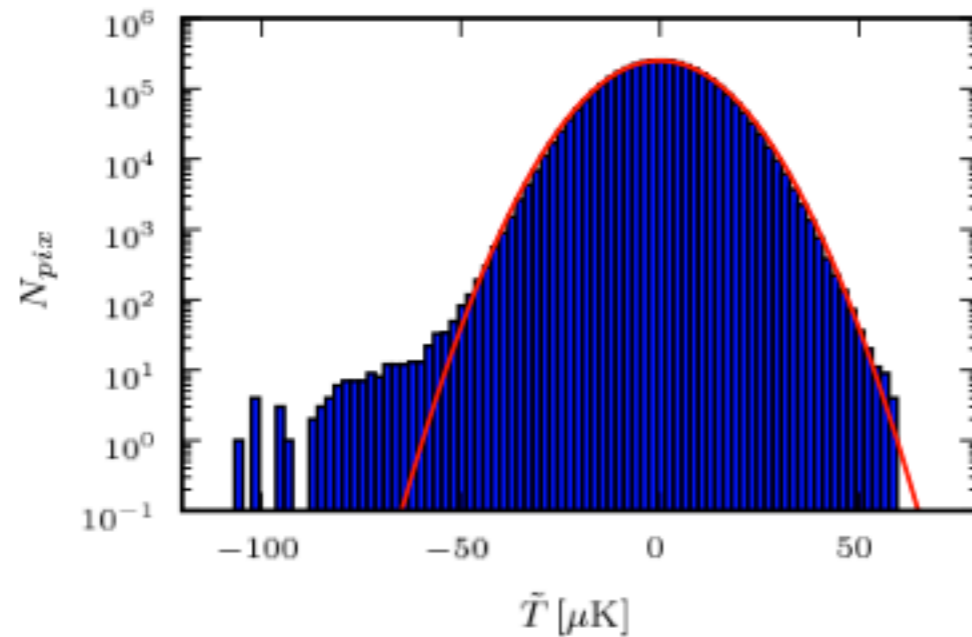
FIG. 2. Histogram of the pixel temperature values in the filtered, masked ACT CMB temperature maps. A Gaussian curve is overlaid in red.

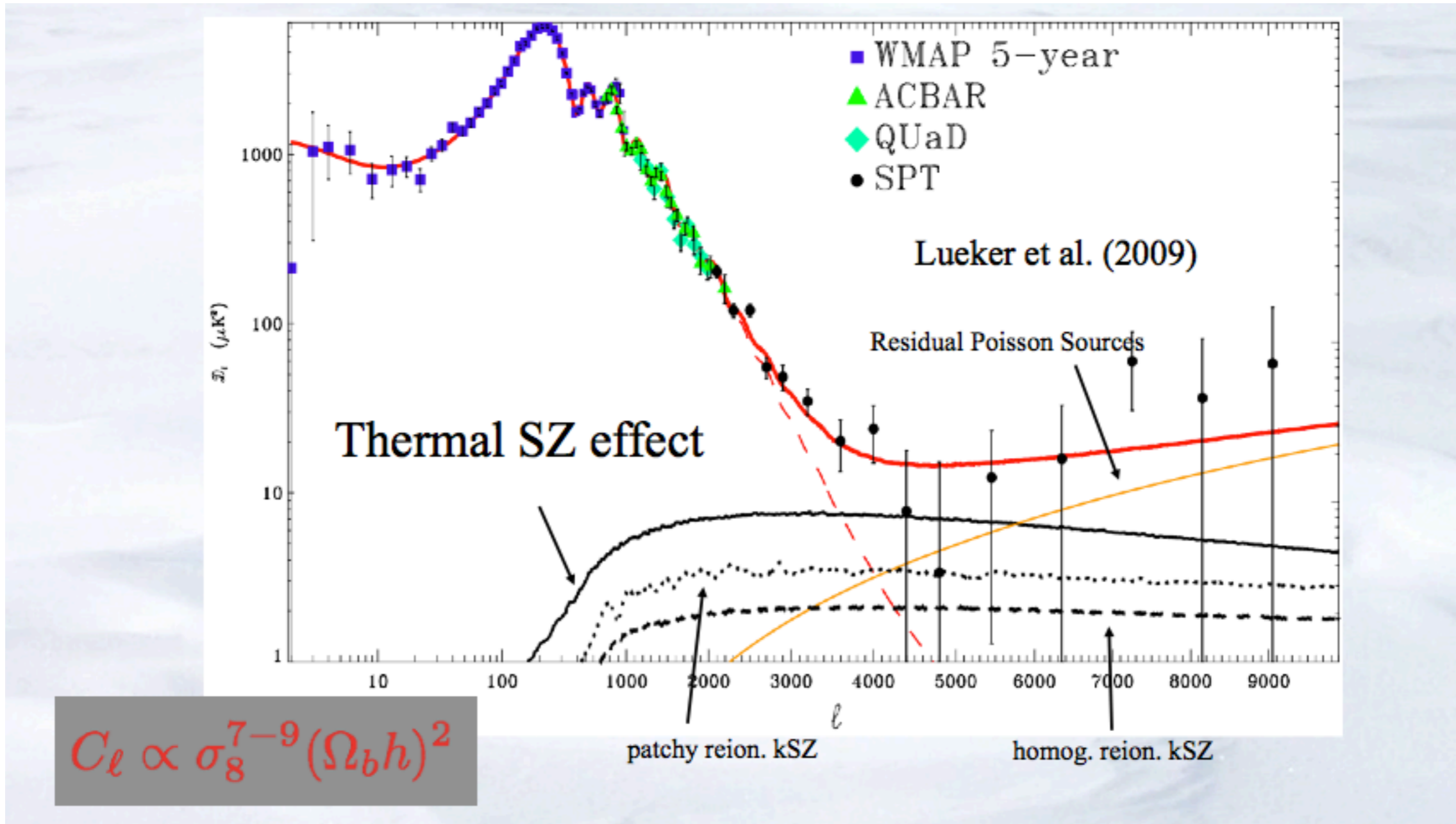FIG. 3. Likelihood of the skewness measurement described in the text (with measurement errors).

$\alpha_3 \sim 10$!!

$$\sigma_8^D = \sigma_8^S \left[\frac{\langle \tilde{T}^3 \rangle^D}{\langle \tilde{T}^3 \rangle^S} \right]^{1/\alpha_3}$$

Value of σ_8 obtained by comparing with simulations.

$$\sigma_8 = 0.76^{+0.03}_{-0.04} \ (68\% \ \text{C.L.}) \ ^{+0.05}_{-0.16} \ (95\% \ \text{C.L.})$$

1D PDF and bispectrum analysis
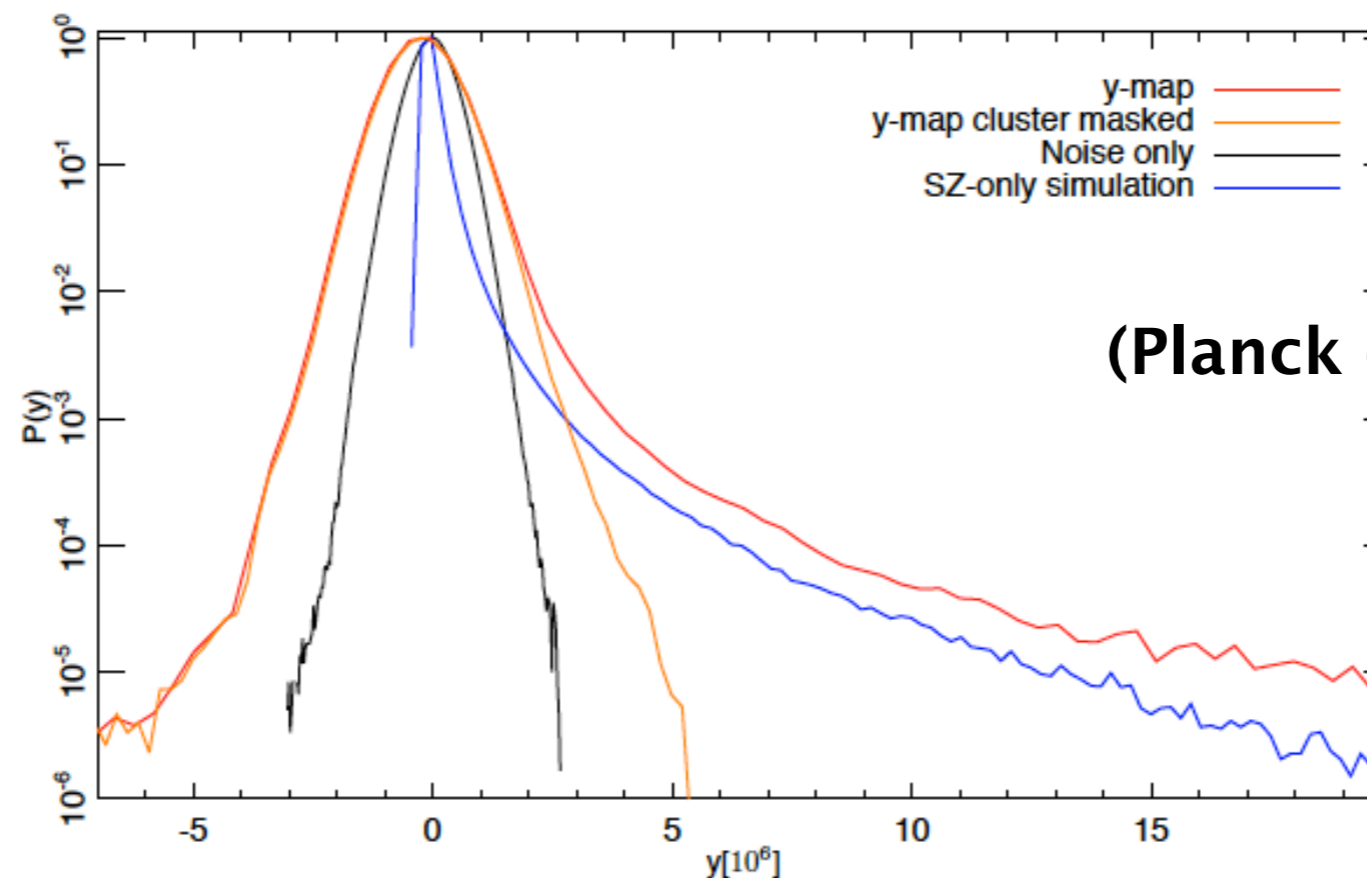
(Planck collaboration 2015)

The tSZ bispectrum is a higher order moment of the anisotropy and measures the deviation from Gaussianity of the signal. The main differences between the model dependence of the bispectrum and the power spectrum are:

- The tSZ bispectrum has a stronger scaling with σ_8 ($D_l \propto \sigma_8^{11\text{-}12}$) than the power spectrum ($D_l \propto \sigma_8^{7\text{-}9}$) (Bhattacharya et al. 2012; Cooray 2000; Rubino-Martin & Sunyaev 2003).

- The tSZ bispectrum is less sensitive to astrophysical uncertainties because it is principally sourced by massive clusters ($M_{500c} \sim 6.5 \times 10^{14}\, h^{-1}\, M_{Sun}$) at intermediate redshift ($z \sim 0.4$) (Bhattacharya et al. 2012), for which the observational data are better. This is in contrast to the SZ power spectrum, which receives significant contributions from less understood low-mass and high-redshift clusters.

(From CCAT White Paper)

Optical observations: velocity dispersion, galaxy richness & lensing

Cluster optical observation: richness
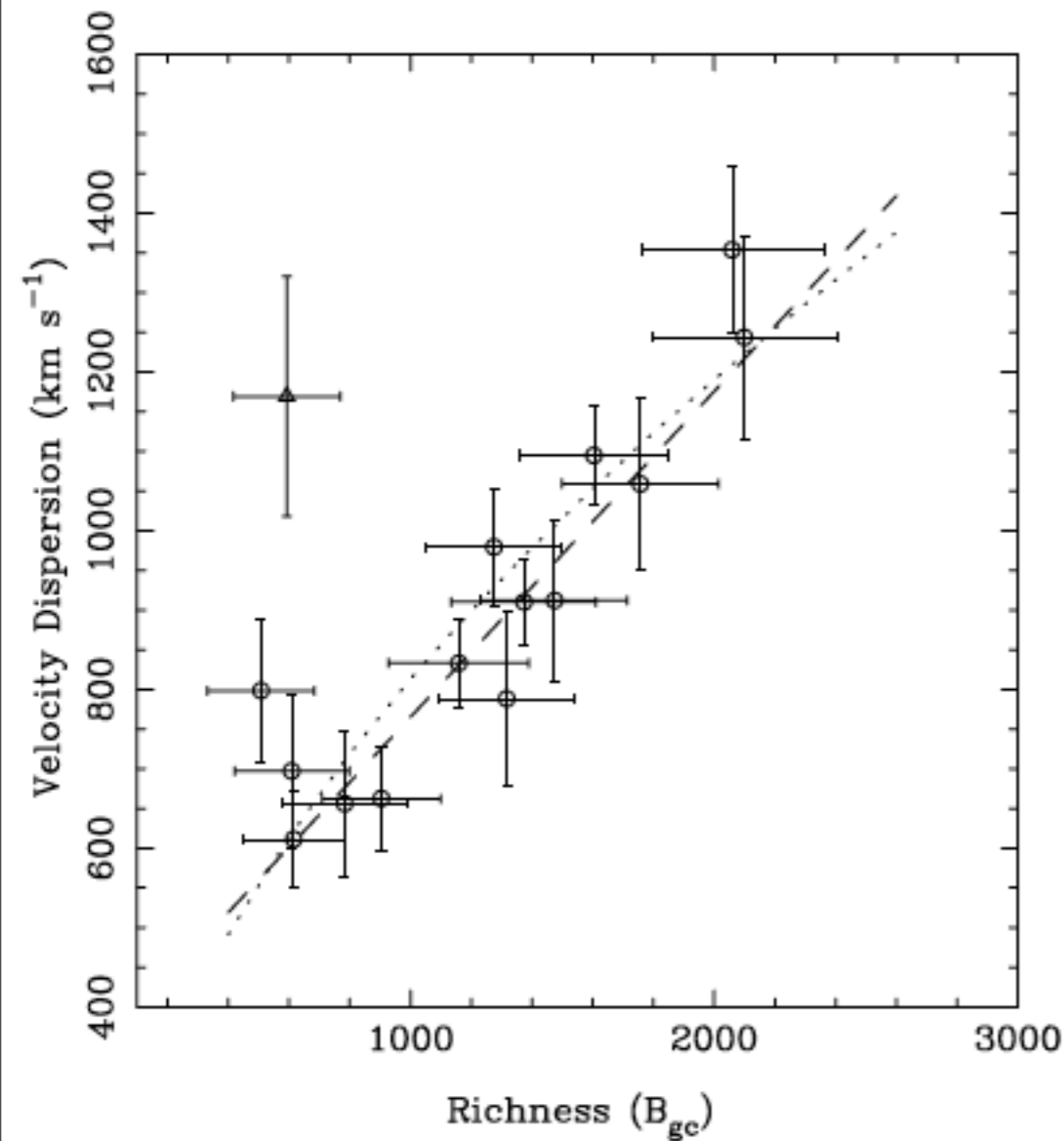
Yee & Ellingson 2003

Clusters in optical surveys are selected on the basis of richness, which depends on the number of galaxies observed within a certain projected radius from the cluster center.

$$\frac{M_{200}}{10^{14} h^{-1} M_{\odot}} = (1.42 \pm 0.08) \left(\frac{N_{200}}{20}\right)^{1.16 \pm 0.09}.$$
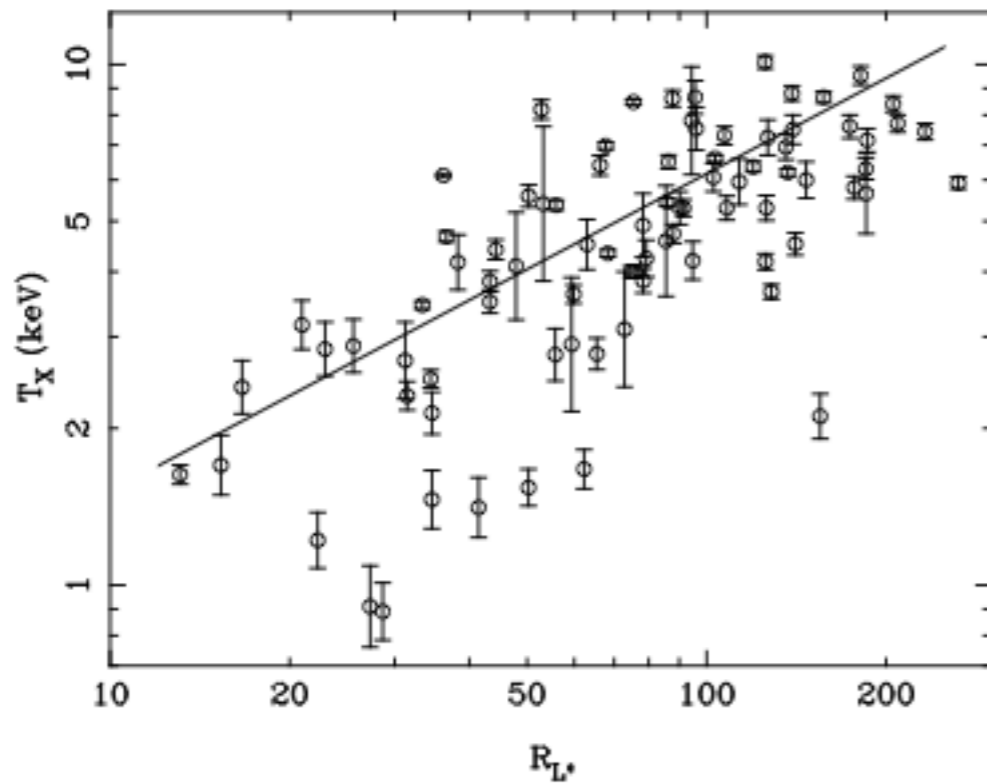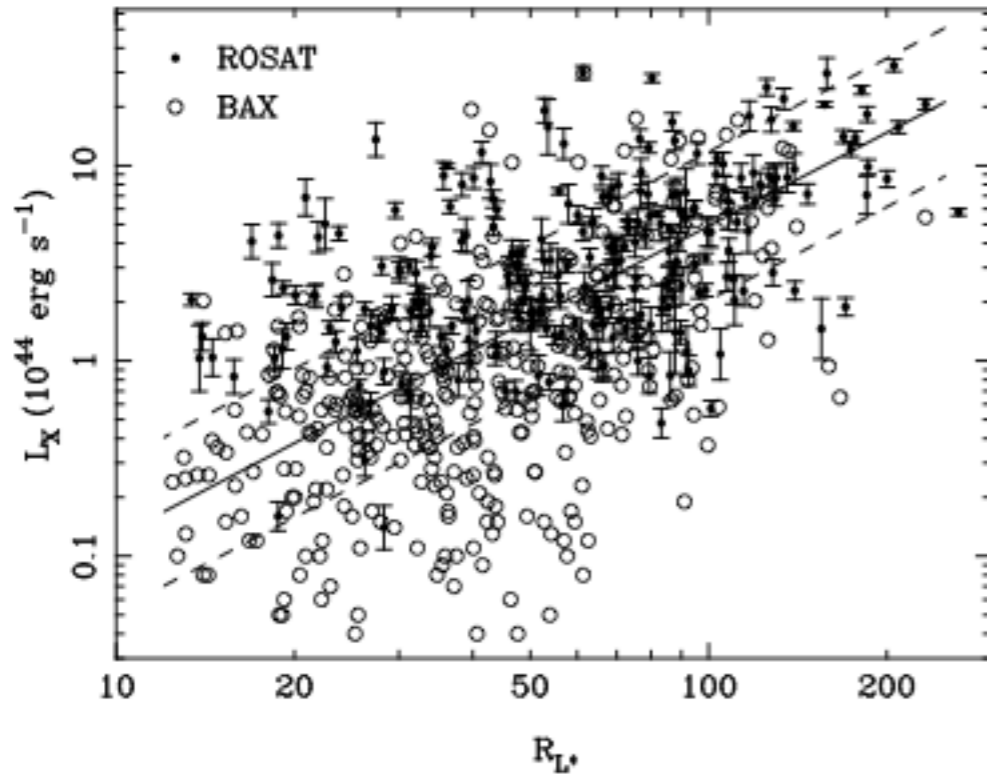
Optical richness

**From SDSS cluster catalog paper
by Wen, Han & Liu (2012)**

FIG. 18. — Correlations between the cluster richness with the SZ measurement by Planck.

SDSS optical cluster catalog

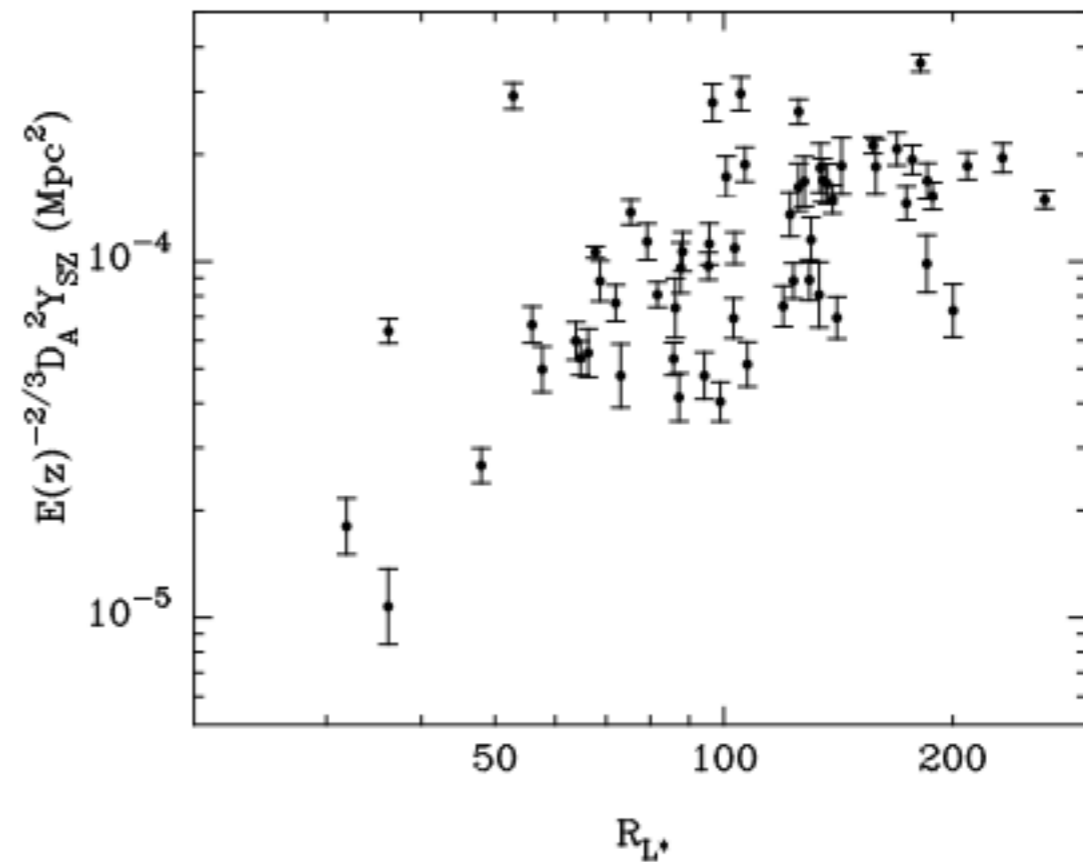A CATALOG OF 132,684 CLUSTERS OF GALAXIES IDENTIFIED FROM SLOAN DIGITAL SKY SURVEY III

Z. L. WEN[1], J. L. HAN[1] AND F. S. LIU[2]

ABSTRACT

Using the photometric redshifts of galaxies from the Sloan Digital Sky Survey III (SDSS-III), we identify 132,684 clusters in the redshift range of $0.05 \leq z < 0.8$. Monte Carlo simulations show that the false detection rate is less than 6% for the whole sample. The completeness is more than 95% for clusters with a mass of $M_{200} > 1.0 \times 10^{14}\ M_\odot$ in the redshift range of $0.05 \leq z < 0.42$, while clusters of $z > 0.42$ are less complete and have a biased smaller richness than the real one due to incompleteness of member galaxies. We compare our sample with other cluster samples, and find that more than 90% of previously known rich clusters of $0.05 \leq z < 0.42$ are matched with clusters in our sample. Richer clusters tend to have more luminous brightest cluster galaxies (BCGs). Correlating with X-ray and the Planck data, we show that the cluster richness is closely related to the X-ray luminosity, temperature, and Sunyaev–Zel'dovich measurements. Comparison of the BCGs with the SDSS luminous red galaxy (LRG) sample shows that 25% of LRGs are BCGs of our clusters and 36% of LRGs are cluster member galaxies. In our cluster sample, 63% of BCGs of $r_{\mathrm{petro}} < 19.5$ satisfy the SDSS LRG selection criteria.

Velocity dispersion

Velocity dispersion is the optical analog of X–ray temperature.

Observationally: $\sigma^2 = (1.0 \pm 0.1) \, k_B \, T_X \, / \, \mu \, m_p$
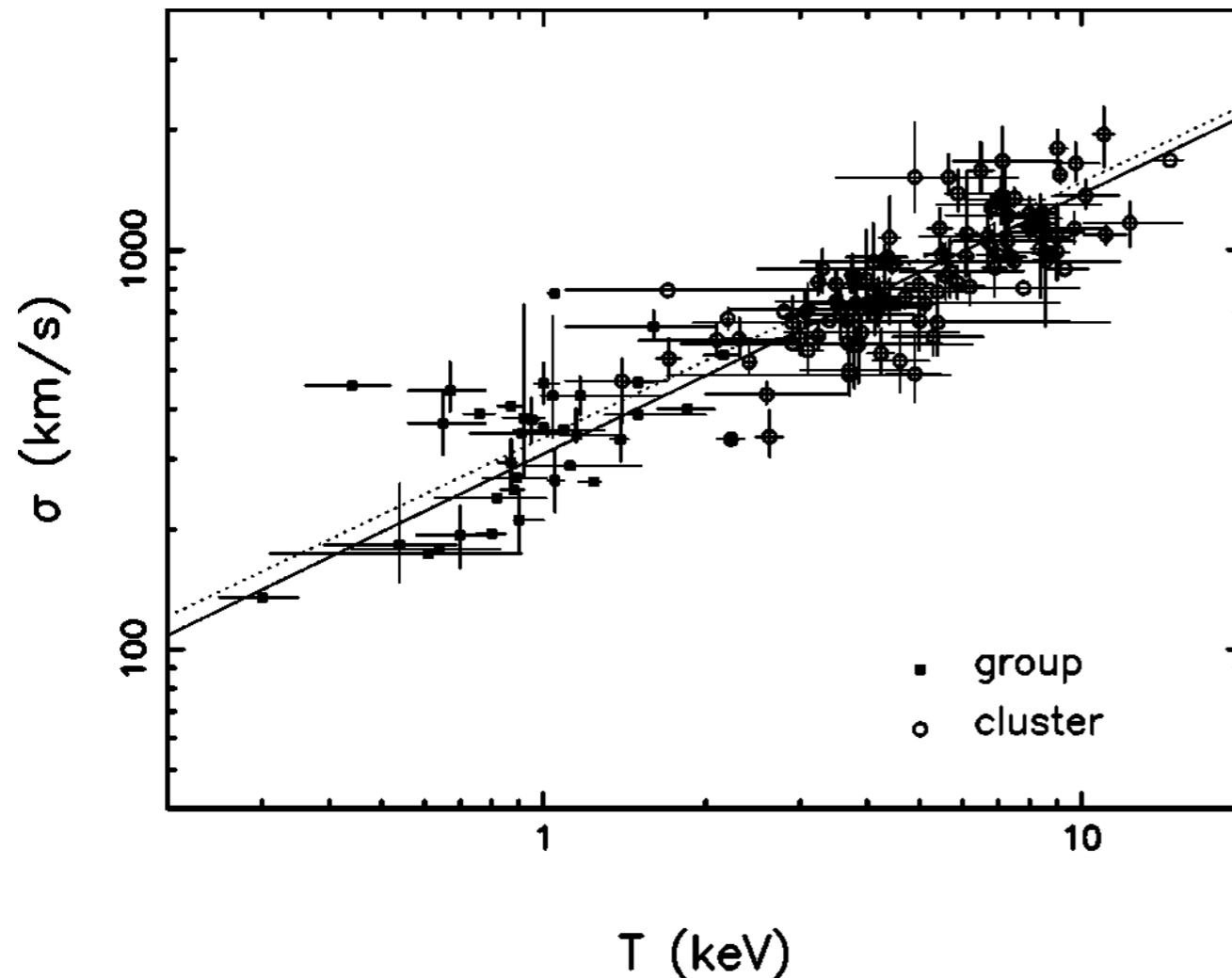
The ratio **$\sigma^2 \, / \, kT_X$** depends on the (logarithmic) slope of the gas density profile to that of the galaxy profile:

$$\frac{\sigma_r^2}{\frac{kT}{\bar{m}}} = \frac{d \ln n_{gas}/d \ln r}{d \ln n_{gal}/d \ln r + 2A}.$$

$$= \frac{d \ln n_{gas}/d \ln r}{d \ln n_{gal}/d \ln r}$$

Deviation of this ratio from unity can indicate the feedback mechanisms affecting the ICM density distribution.

Problem with velocity dispersions
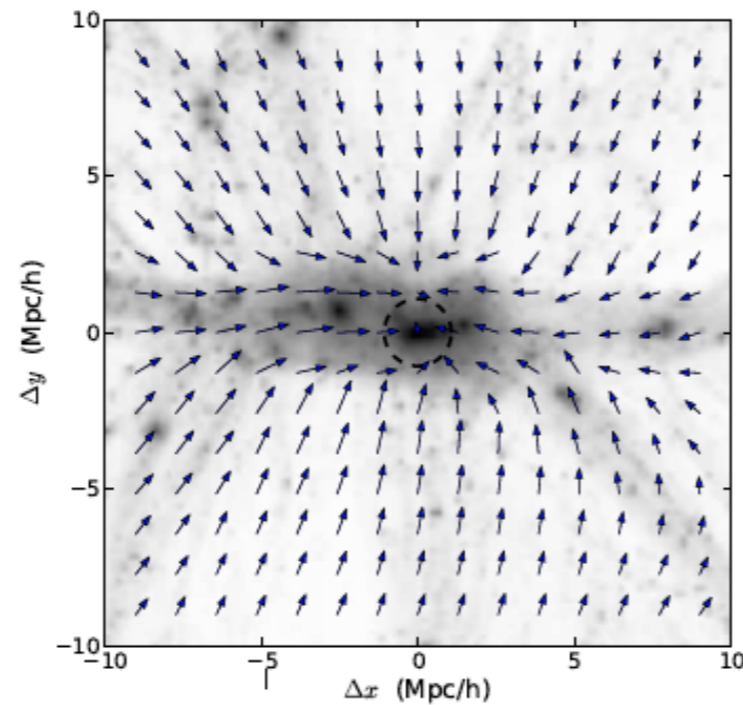
The velocity field traces the filamentary substructure
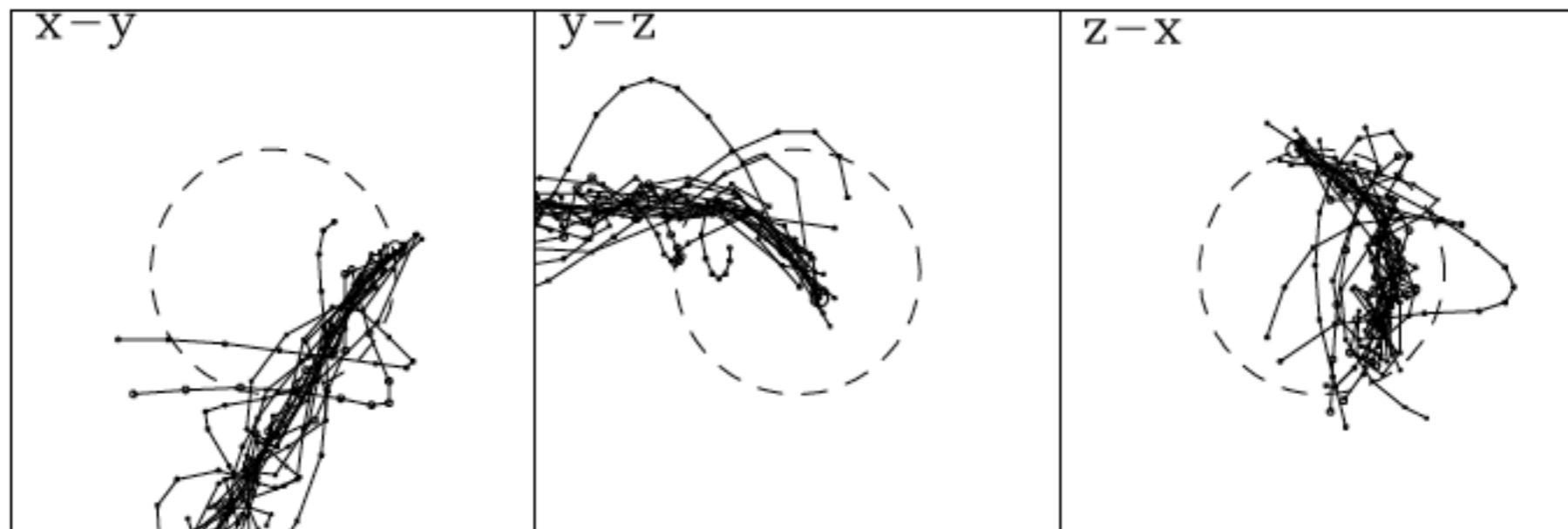
Persistence of substructures (simulations by White, Cohn & Smit 2010)

Dynamical mass example
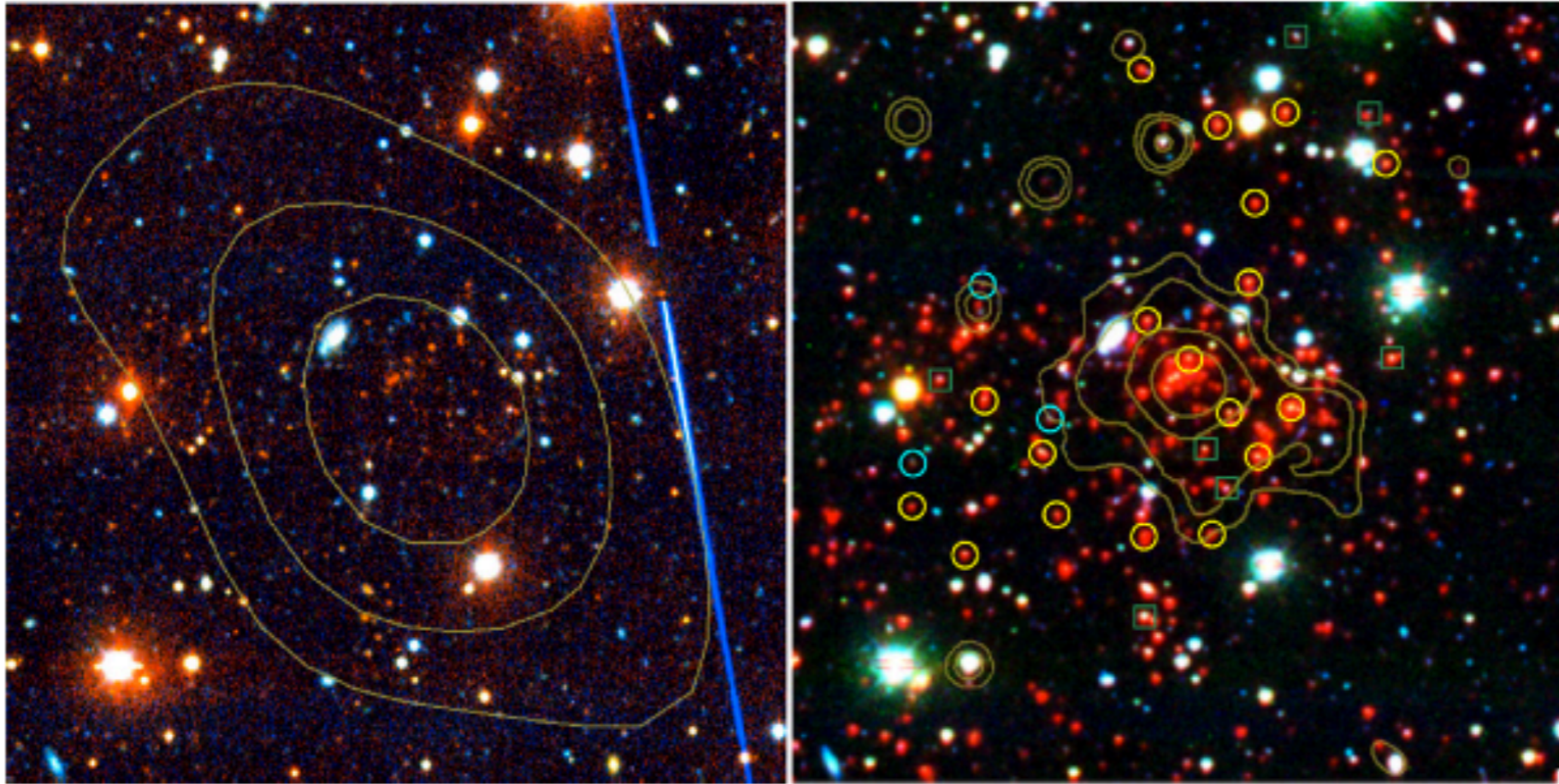
Figure 1. Left: optical $4' \times 4'$ color image (grz) of SPT-CL J0546-5345, with SZE significance contours overlaid (S/N = 2, 4, and 6). Right: false color optical (ri)+IRAC (3.6 μm) image of SPT-CL J0546-5345, with *Chandra* X-ray contours overlaid (0.25, 0.4, 0.85, and 1.6 counts per $2'' \times 2''$ pixel per 55.6 ks in the 0.5–2 keV band). North is up, east is to the left. Due to its high angular resolution, *Chandra* is able to resolve substructure to the SW, which may be evidence of a possible merger. These images highlight the importance of IRAC imaging in studying the galaxies in high-redshift, optically faint clusters. Spectroscopic early-type (late-type) members are indicated with yellow (cyan) circles. Green squares show the spectroscopic non-members.

Dynamical mass example
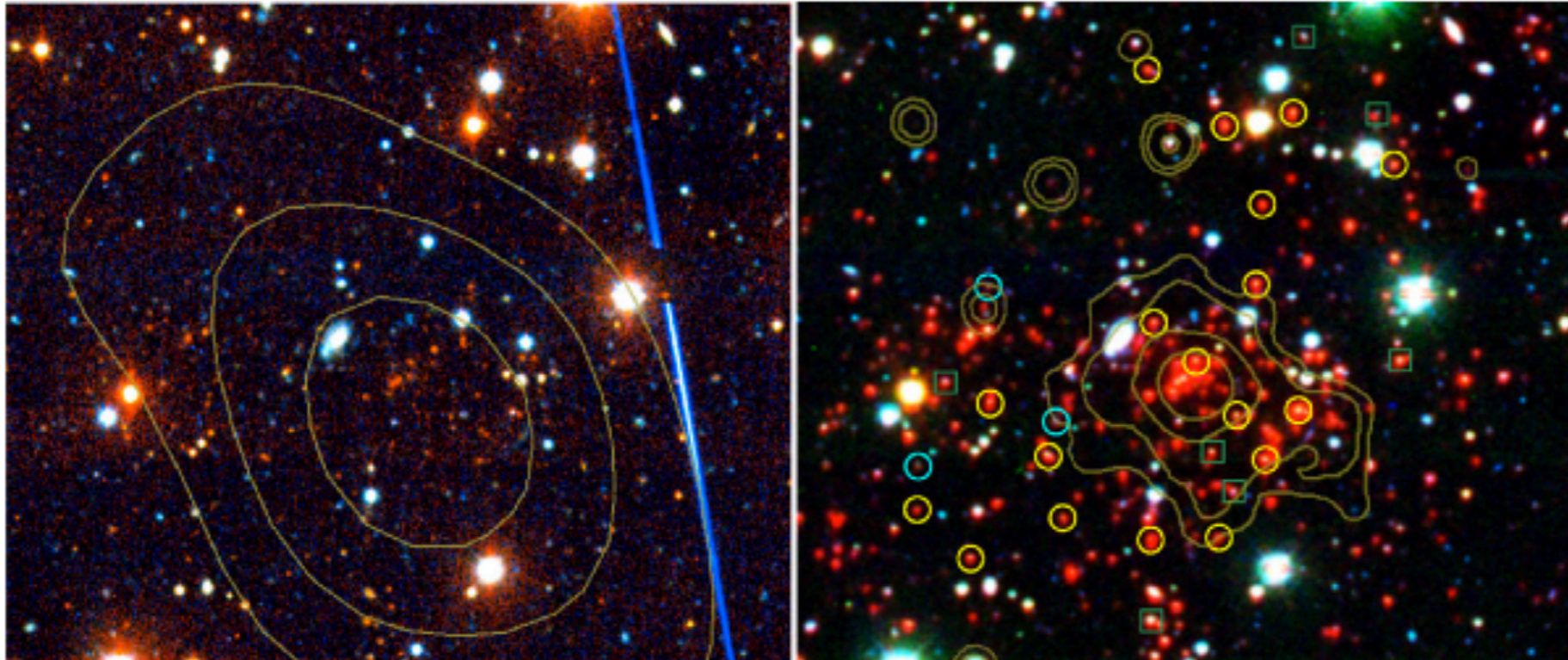
Comparison of Mass Measurements for SPT-CL J0546-5345

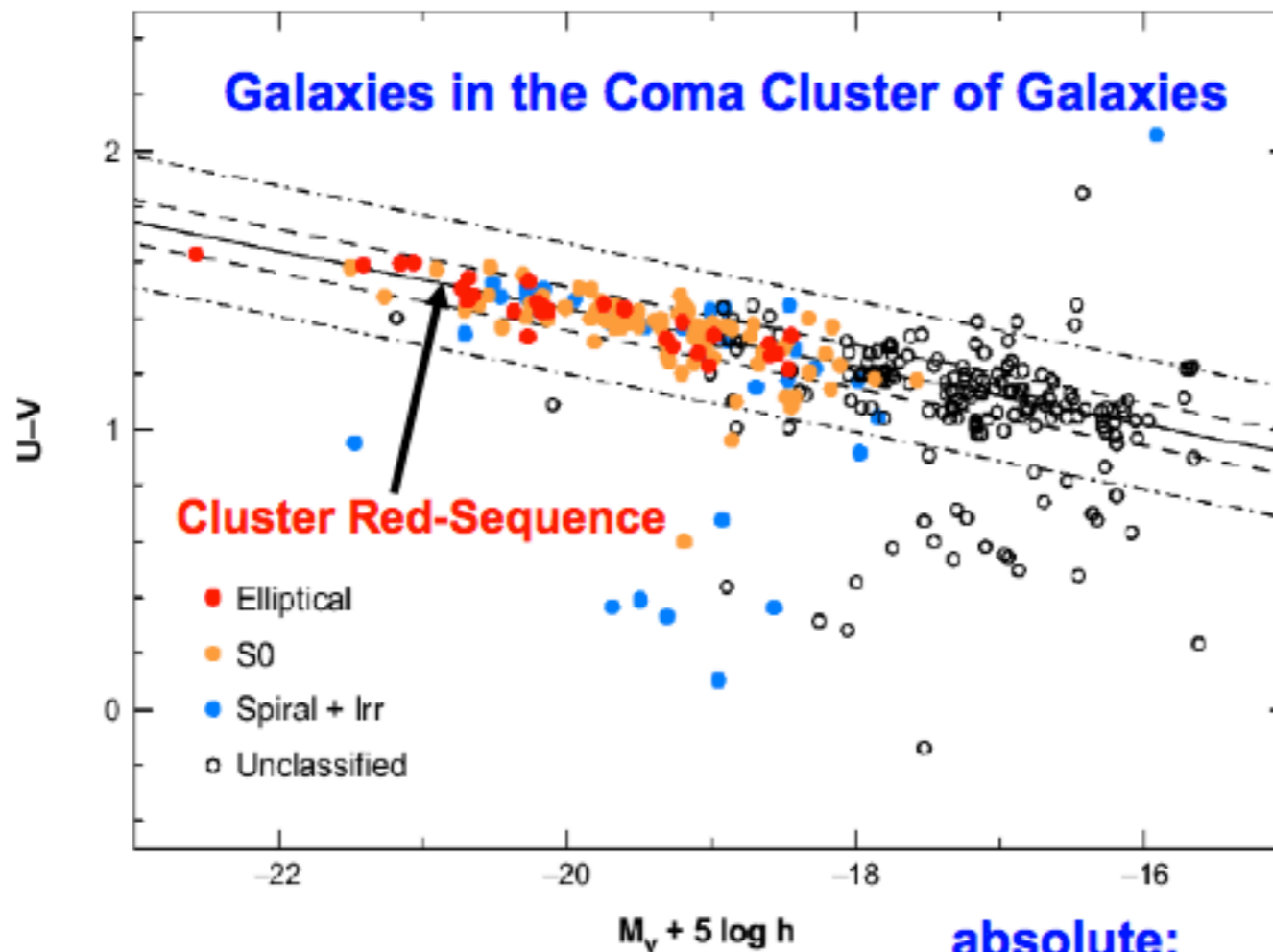| Mass Type	Proxy	Measurement	Units	Mass Scaling Relation	M_{200}[a,b] $(10^{14}\, M_\odot)$
Dispersion	**Biweight**	1179^{+232}_{-167}	km s^{-1}	$\sigma - M_{200}$ (Evrard et al. 2008)	$\mathbf{10.4^{+6.1}_{-4.4}}$
	Gapper	1170^{+240}_{-128}	km s^{-1}	$\sigma - M_{200}$ (Evrard et al. 2008)	$10.1^{+6.2}_{-3.3}$
	Std deviation	1138^{+205}_{-132}	km s^{-1}	$\sigma - M_{200}$ (Evrard et al. 2008)	$9.3^{+5.0}_{-3.2}$
X-ray	Y_X	5.3 ± 1.0	$\times 10^{14}\, M_\odot$ keV	$Y_X - M_{500}$ (Vikhlinin et al. 2009)	$\mathbf{8.23 \pm 1.21}$
	T_X	$7.5^{+1.7}_{-1.1}$	keV	$T_X - M_{500}$ (Vikhlinin et al. 2009)	8.11 ± 1.89
SZE	Y_{SZ}	3.5 ± 0.6	$\times 10^{14}\, M_\odot$ keV	$Y_{SZ} - M_{500}$ (A10)	$\mathbf{7.19 \pm 1.51}$
	S/N at 150 GHz	7.69		$\xi - M_{500}$ (V10)	$5.03 \pm 1.13 \pm 0.77$
Richness	N_{200}	80 ± 31	Galaxies	$N_{200} - M_{200}$ (H10)	$\mathbf{8.5 \pm 5.7 \pm 2.5}$
	N_{gal}	66 ± 7	Galaxies	$N_{gal} - M_{200}$ (H10)	$9.2 \pm 4.9 \pm 2.7$
Best	**Combined**				$\mathbf{7.95 \pm 0.92}$

Figure 1
(ri) + IR
0.5–2 ke
possible
(late-typ

optical
in the
e of a
y-type

Photometry of clusters

The Color-Magnitude-Diagram (CMD)

as basic tool for the study of galaxy evolution in galaxy clusters

Galaxies in the Coma Cluster of Galaxies

Cluster Red-Sequence

- Elliptical
- S0
- Spiral + Irr
- Unclassified

$M_V + 5 \log h$

Source: Bower et al. 1989

the **brighter** a galaxy
→the farther on the **left**

the **redder** a galaxy
→the farther **up** in the CMD

the pronounced locus
(Häufungslinie) of early-type
galaxies (E+S0) is called
Red-Sequence

absolute: $M_X - M_Y$ vs M_Y
observed: $m_X - m_Y$ vs m_Y
$M = M(M_{stellar}, Z, SF\text{-}history, dust,…)$
$m = m(z, K_{cor}, M_{stellar}, Z, SF\text{-}history, dust,…)$

Red sequence technique

- a **pronounced red-sequence** in the CMD is a basic cluster characteristic and is present for basically all known clusters up to high-z

- red-sequence galaxies **selected with appropriate color-cuts** in the CMD give a high contrast of cluster members relative to background or foreground galaxies (interlopers)

- the identification of a red-sequence with an appropriate filter combination is an **efficient method** for the optical/IR search for distant clusters or the photometric confirmation of X-ray selected candidates

- the redshift evolution of the red-sequence in the CMD (mean color/ zero point, RS slope, scatter) is a powerful tool to study early-type galaxy formation and evolution in clusters

- the homogeneous color properties and redshift evolution of the RS galaxies suggest a common underlying formation mechanism

Red sequence technique

The red-sequence technique is uses the fact that all galaxy clusters, however they were discovered, possess a population of galaxies which exhibit a tight relationship in color—magnitude space, the red-sequence.

The red-sequence method involves constructing many colour slices from the survey data and searching for overdensities of galaxies in these slices. Once significant overdensities are found, the slice containing the peak signal for the overdensity gives the cluster candidate's most probable redshift.
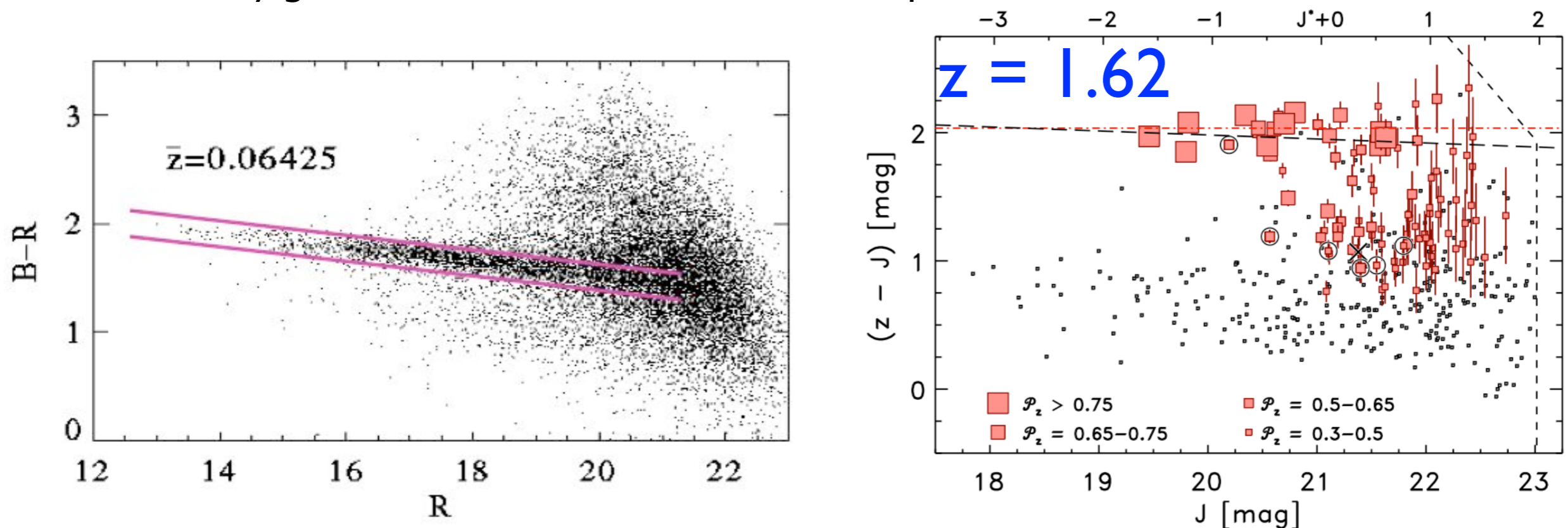
Requires only 2 filters (at minimum): inexpensive
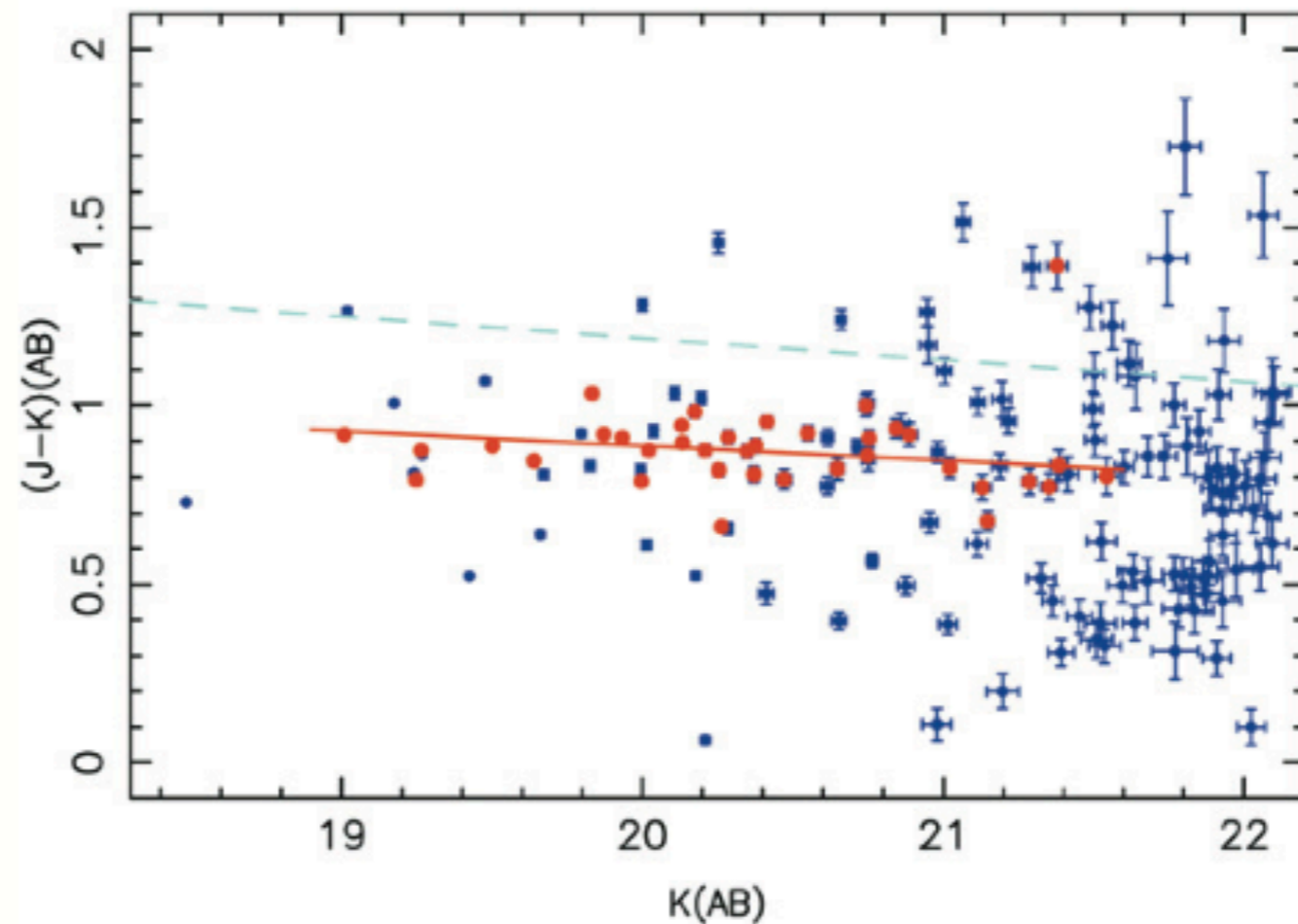
Example: red sequence galaxies

Figure 2: IJK colour composite image of the field centred on RCS0439.6-2905. North is up and East to the left. This image shows approximately the central 1.1 × 1.1 Mpc.

Credit: Barrientos et al., RCS survey

Example: red sequence galaxies

Figure 3: IR colour-magnitude diagram in the field of RCS0439.6-2905. All the objects are included and shown as filled circles. The morphologically selected E/S0 galaxies are shown as open circles. These galaxies define a tight sequence, similar to that found in local clusters. The solid line shows the best fit to the sequence of E/S0 galaxies in the cluster. The broken line corresponds to the colour-magnitude relation for the E/S0 galaxies in Coma cluster redshifted to $z = 0.97$.

Red-sequence Cluster Survey

The Red Sequence Cluster Survey 2

- The Red Sequence Cluster Survey 2 (RCS2) is the largest systematic search for galaxy clusters ever undertaken. Using the square-degree imager, MegaCam, on the CFHT, we are imaging nearly 1000 square degrees of sky in three filters (g', r', z') in order to find clusters out to $z \sim 1$. The project uses the ubiquitous red-sequence of cluster early-type galaxies to identify clusters with a well-understood selection function. This technique was used with great success in the 90 square degree R and z survey, RCS1.

Main Science Goals: (RCS2)
 - Constrain cosmological parameters
   Ω_m (to ~0.03), σ_8 (to ~0.05), w
 - create a sample of ~150 strong lenses
 – cluster evolution
 – weak lensing, cosmic shear (wide/shallow)
 – a very large sample of photo-z
      (useful 0.1<z<0.7)

Cluster sample:
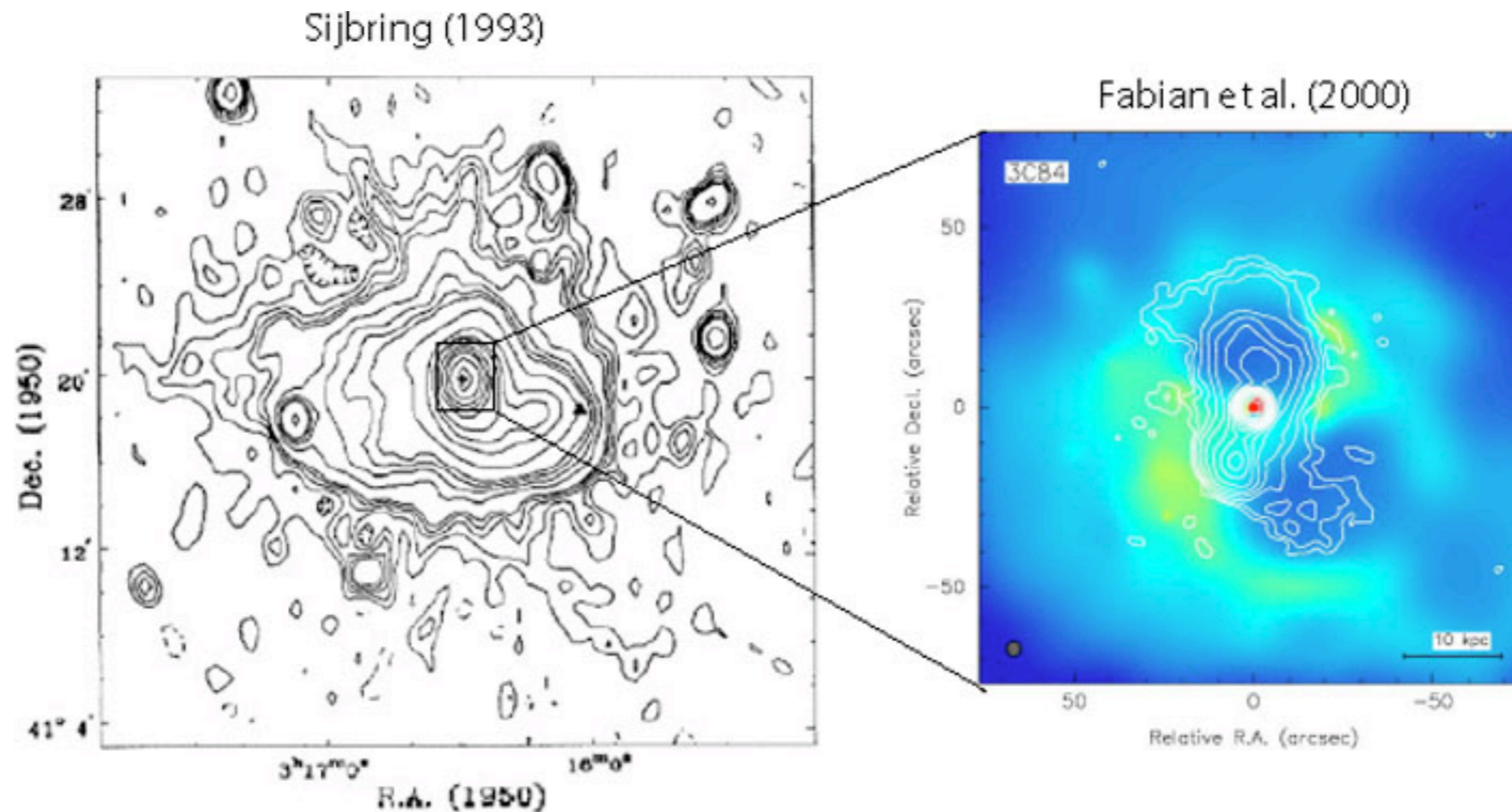 – optimized for z~0.1 to 1.0;
 Total number of clusters (useful
 for cosmology) expected: ~ 15,000 (>~ 2x10^{14})
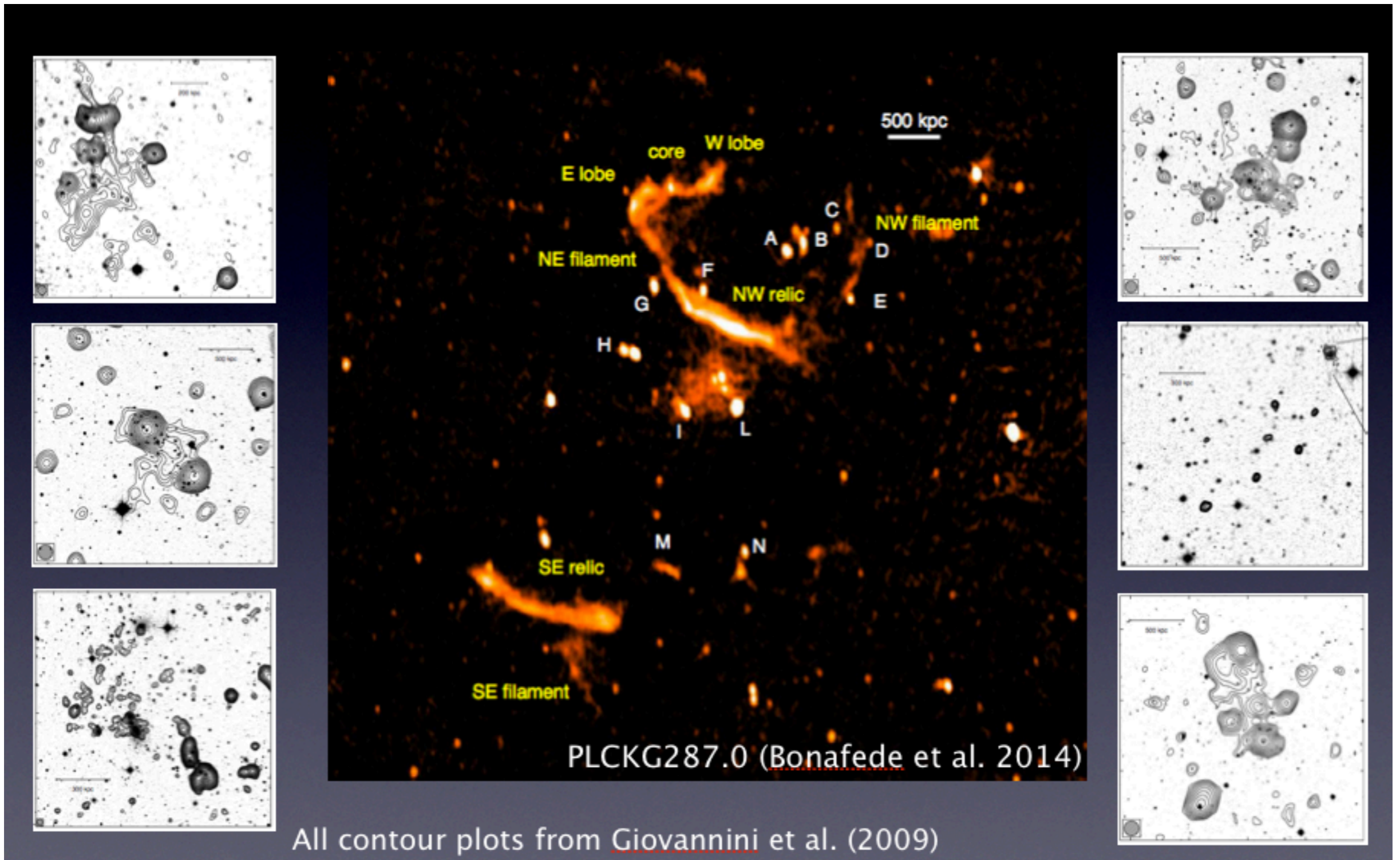
Radio & Gamma-ray observation of clusters

Radio observation of clusters

While the thermal gas emitting in X-rays is present in all clusters, the detection of extended radio emission only in ~10% of the systems indicates that the non-thermal plasma is not a common property of galaxy clusters. Non-thermal emissions over ~1 Mpc scales are present only in the most massive merging systems.
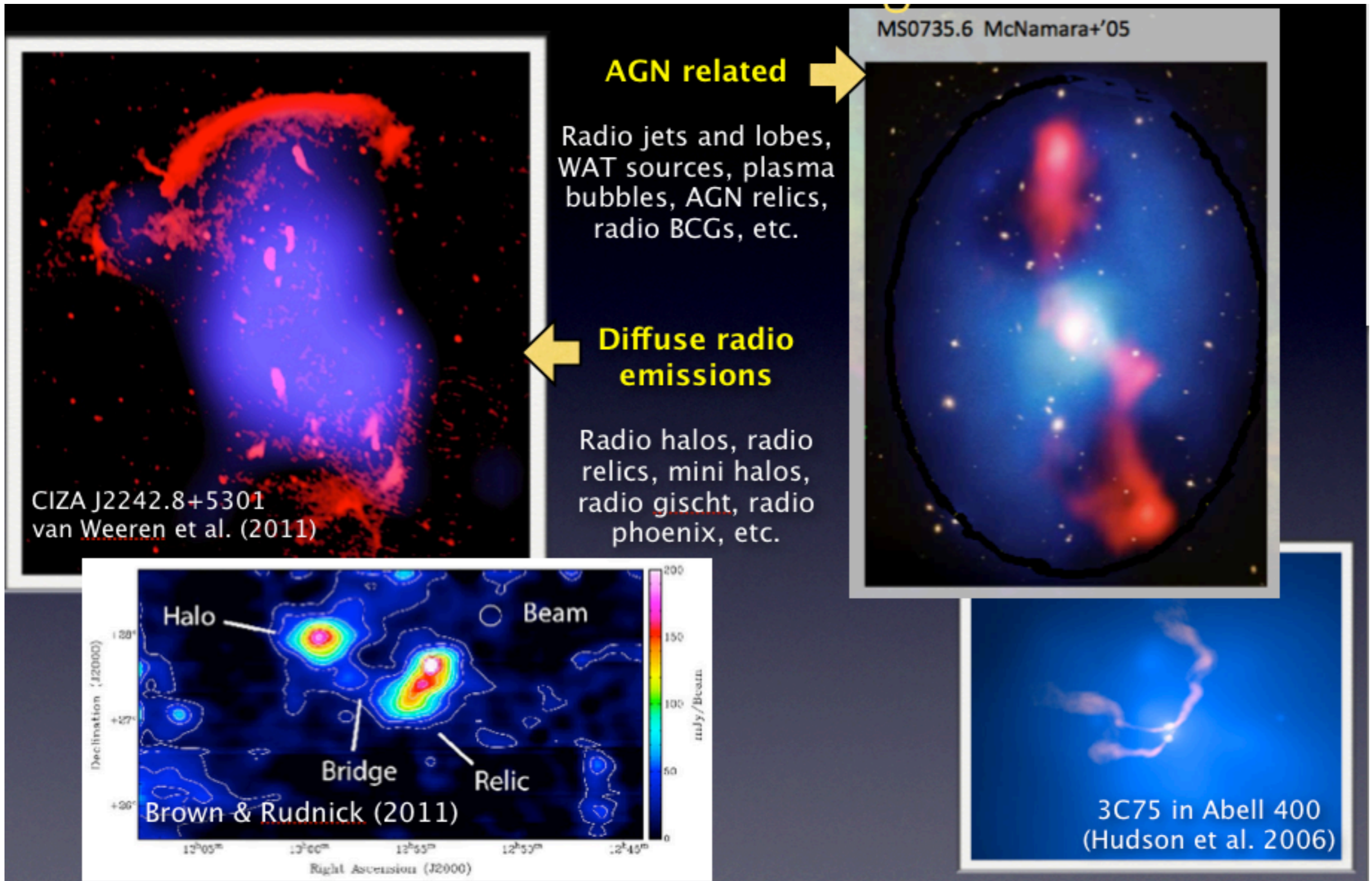

327 MHz map of the mini–halo in the Perseus cluster (z = 0.018).
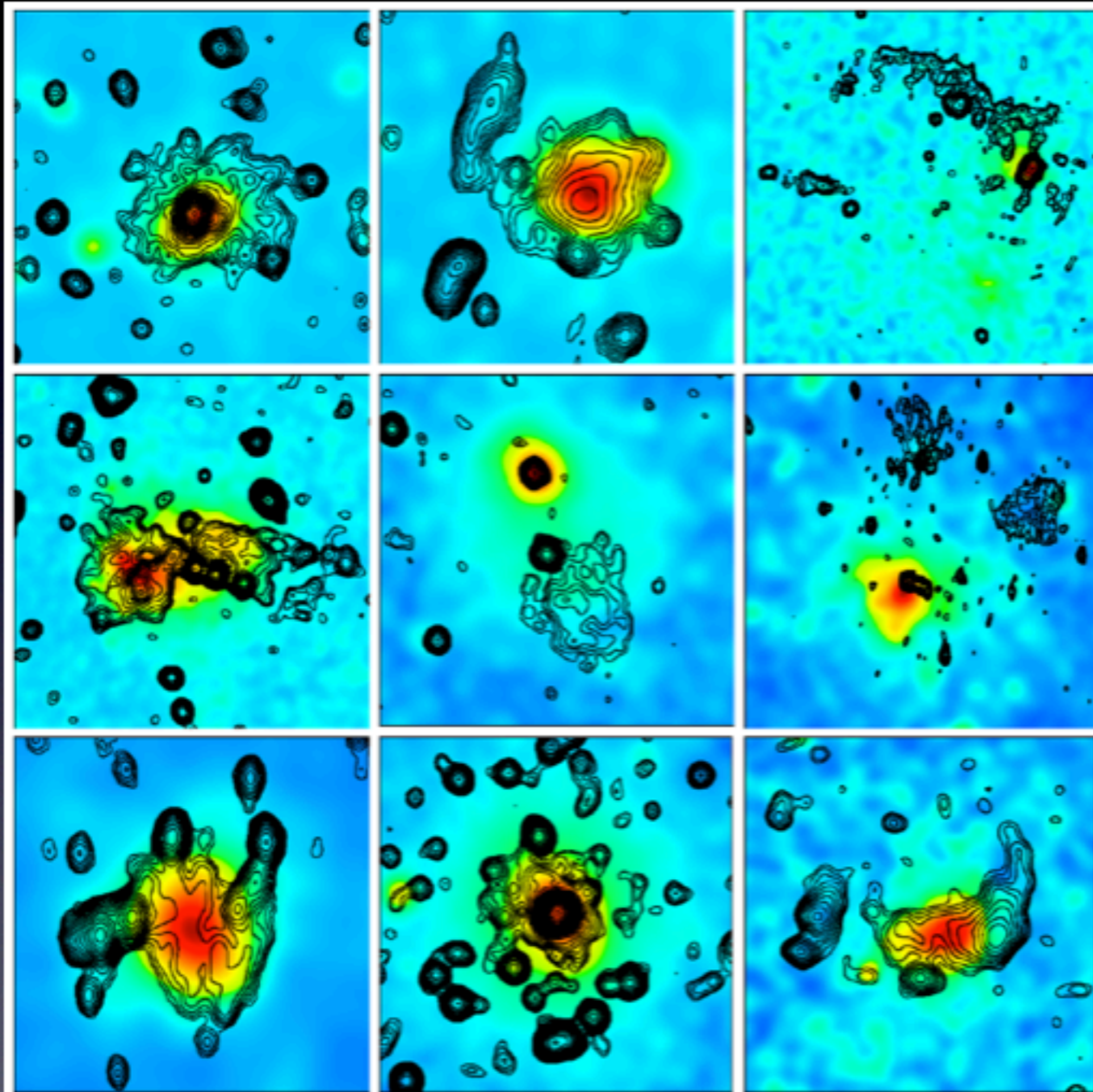
Radio emission in clusters

500 kpc

W lobe
core
E lobe
C
NW filament
A
B
NE filament
D
F
NW relic
G
E
H
I
L
M
N
SE relic
SE filament

PLCKG287.0 (Bonafede et al. 2014)

All contour plots from Giovannini et al. (2009)

Radio emission in clusters

AGN related

Radio jets and lobes, WAT sources, plasma bubbles, AGN relics, radio BCGs, etc.

Diffuse radio emissions

Radio halos, radio relics, mini halos, radio gischt, radio phoenix, etc.

MS0735.6 McNamara+'05

CIZA J2242.8+5301
van Weeren et al. (2011)

Halo   Beam
Bridge   Relic
Brown & Rudnick (2011)

3C75 in Abell 400
(Hudson et al. 2006)

Radio emission in clusters

Gallery taken from Feretti et al. (2012) *Color → X-ray*

Radio halos: $L_{1.4\ GHz} \sim 10^{24-25}$ W/Hz

● Mpc scale diffuse sources near cluster centers
● Low surface brightness and generally not polarized
● Mostly steep spectrum ($\alpha \sim 1.2$)
● Morphology roughly similar to X–ray or SZ emission, no severe projection bias

Radio relics: $L_{1.4\ GHz} \sim 10^{23-25}$ W/Hz

● Mpc scale elongated sources near cluster periphery
● Higher surface brightness and polarized
● Also steep spectrum ($\alpha \sim 1.2$)
● Morphology resembles shock fronts, subject to projection bias

Radio halos in clusters
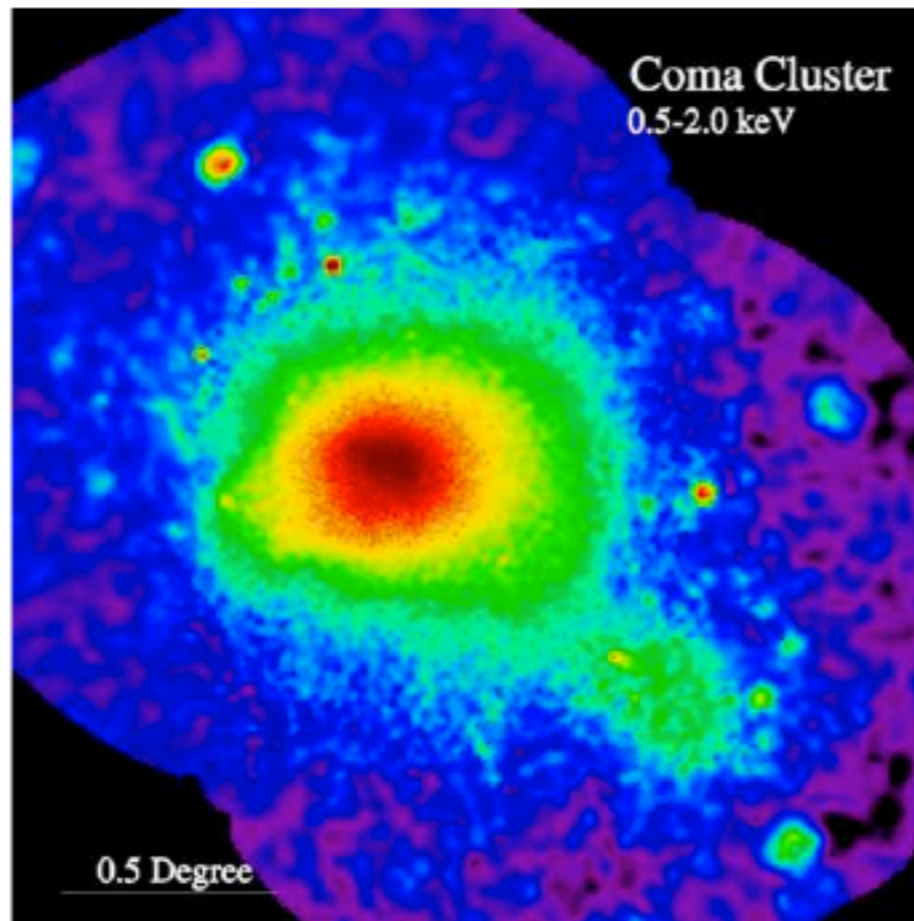
thermal X-ray emission

(Snowden/MPE/ROSAT)
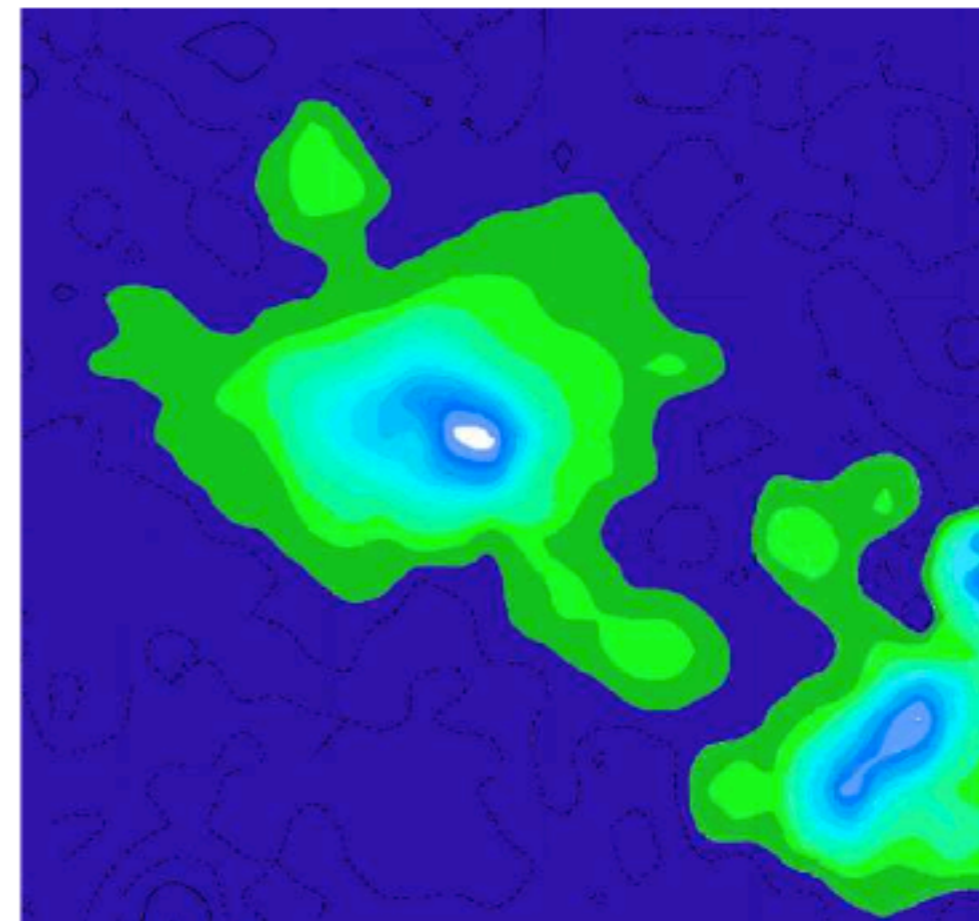
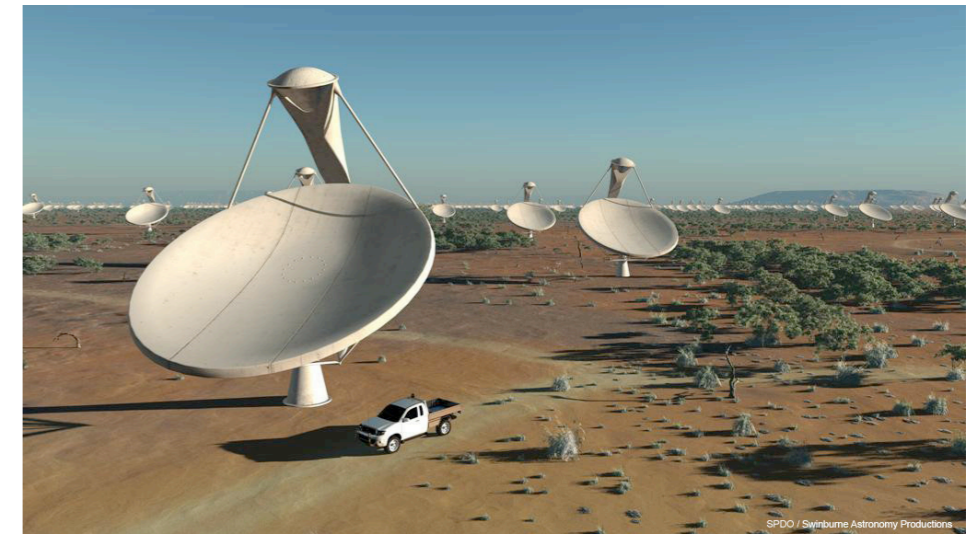radio synchrotron emission

(Deiss/Effelsberg)

How many radio halos in the sky?

We don't know!
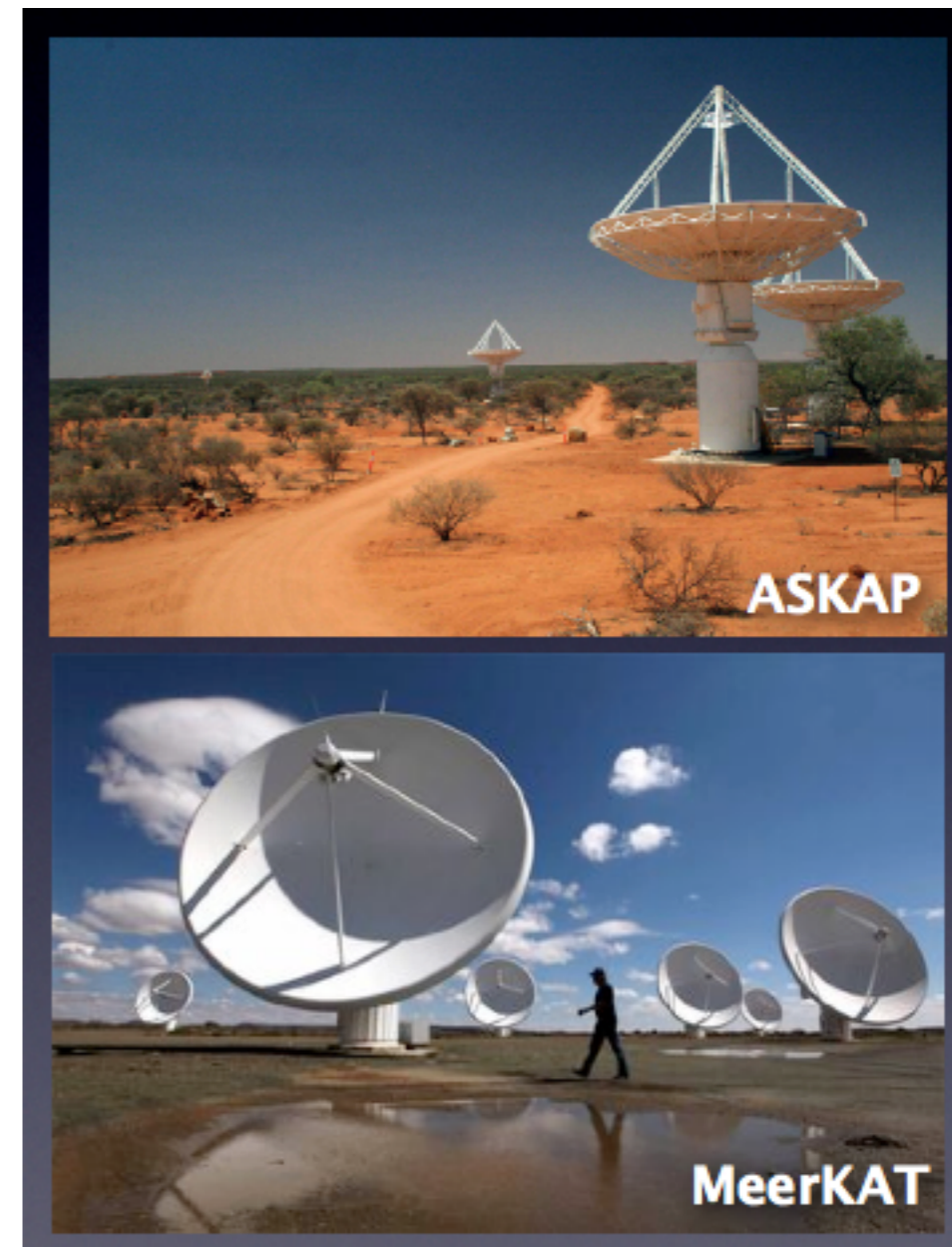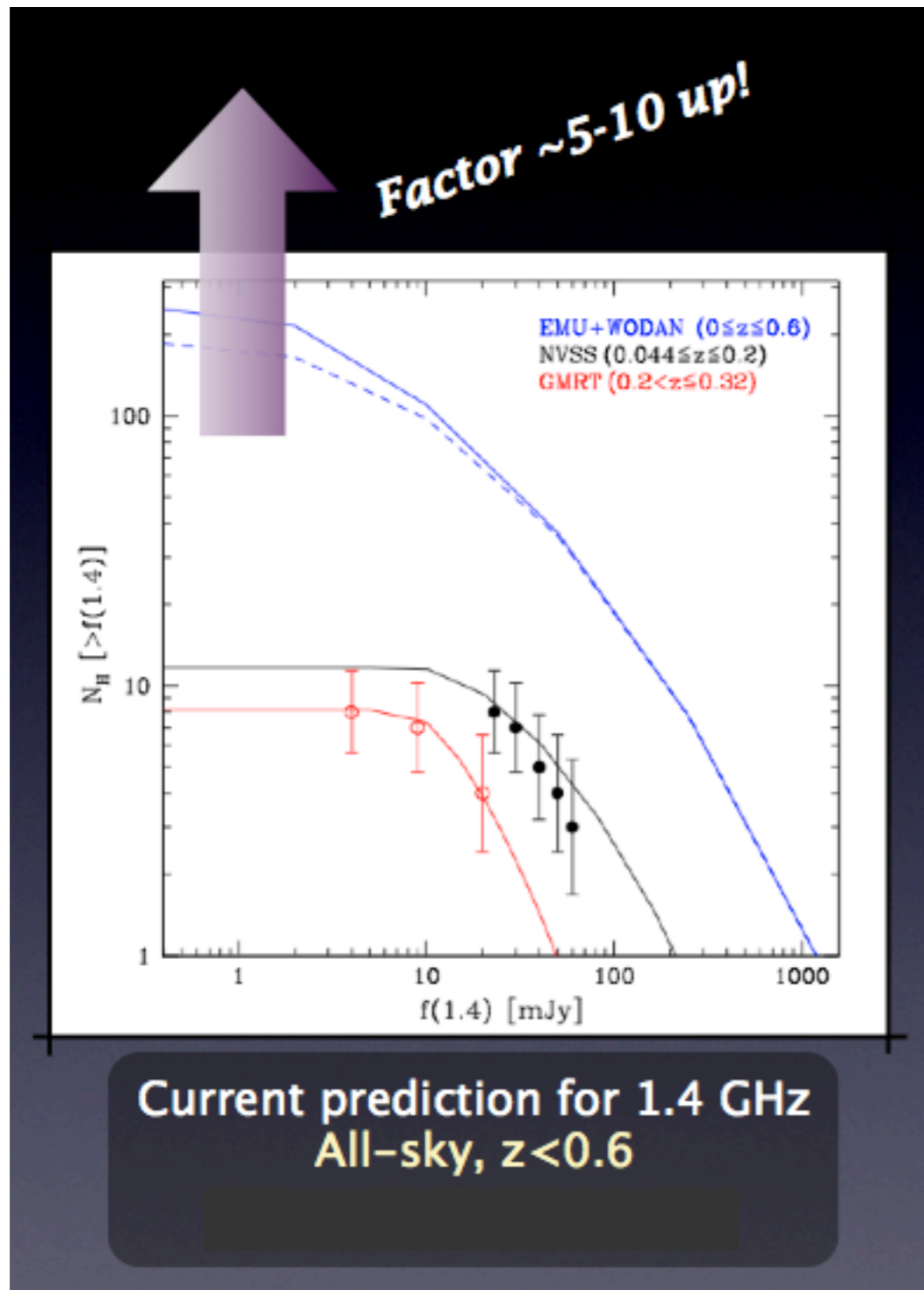
Square Kilometer Array

The Square Kilometre Array (SKA) is a radio telescope project to be built in Australia and South Africa which would have a total collecting area of approximately one square kilometre. It will operate over a wide range of frequencies and its size will make it 50 times more sensitive than any other radio instrument.

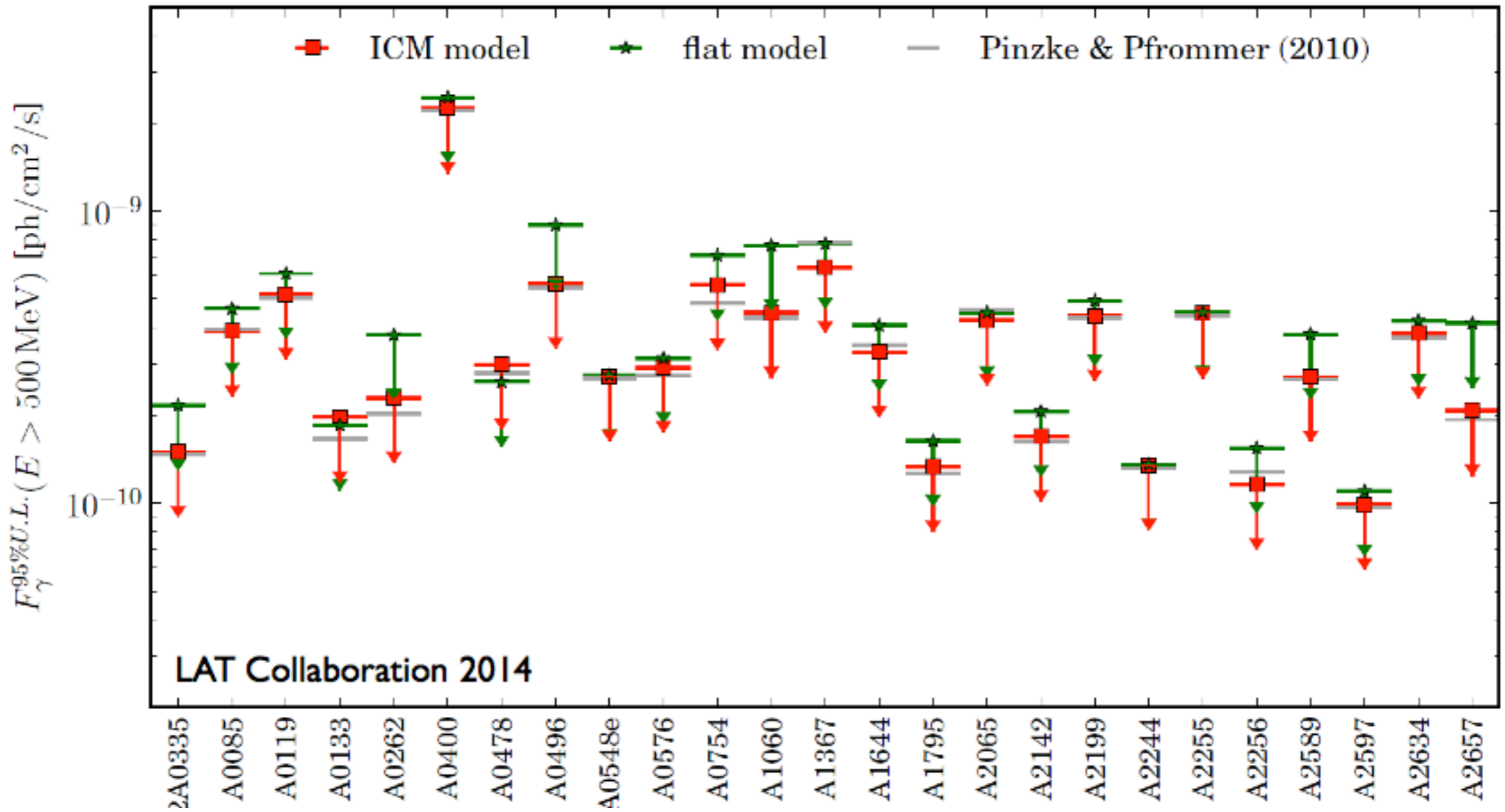(From Wikipedia)

Gamma–ray prediction

Cluster cosmological simulations of *Pfrommer et al. (2008)* and *Pinzke & Pfrommer (2010)* reproduce the observed synchrotron radio (mini-)halo emission and predict the gamma-ray emission. The dominant component results from CR hadronic interactions.
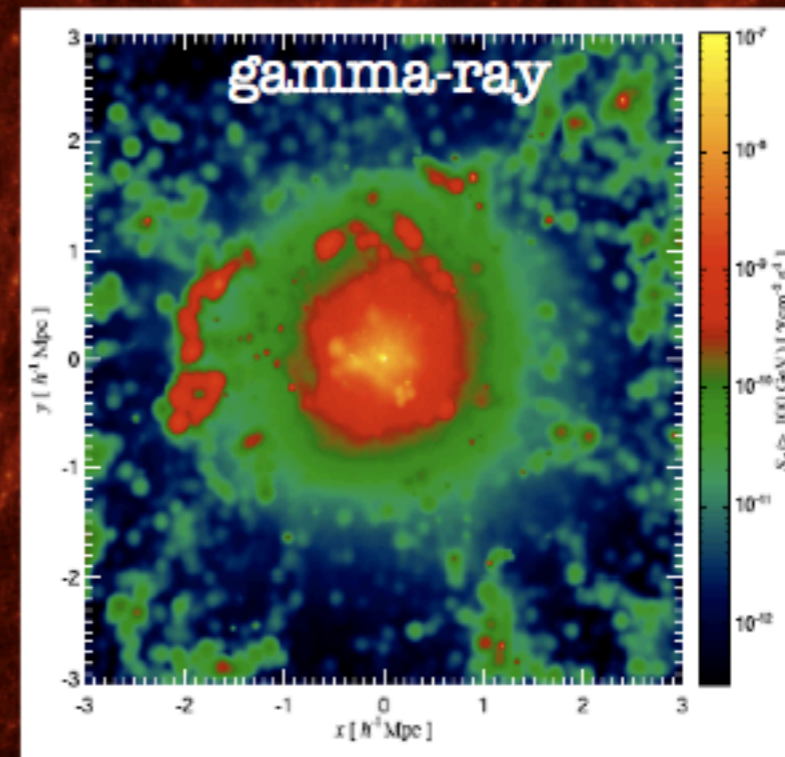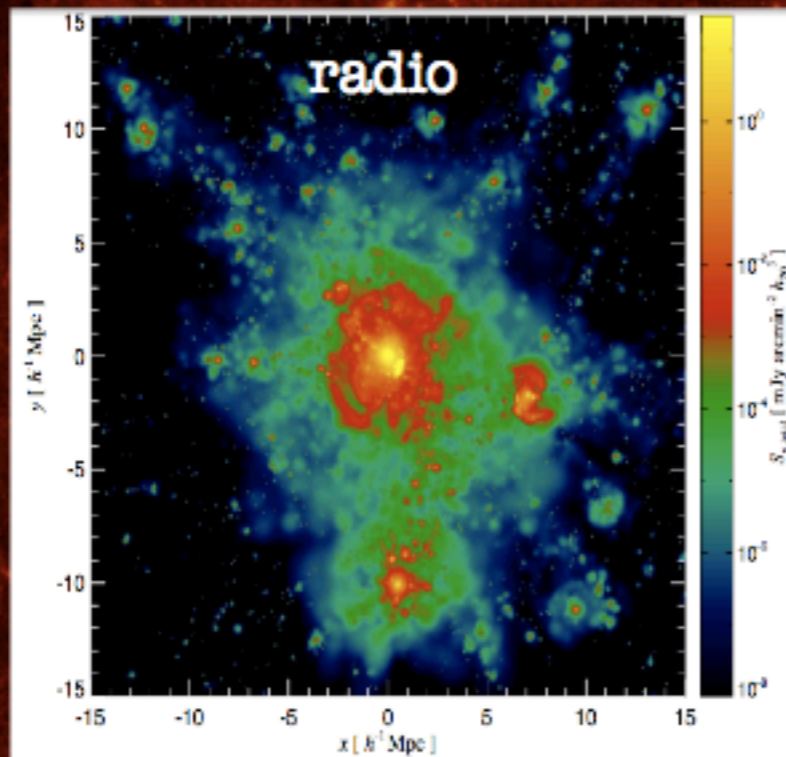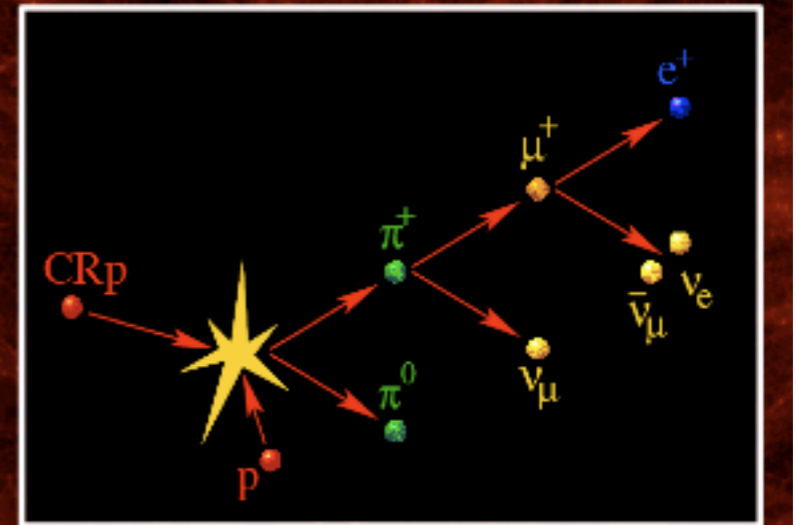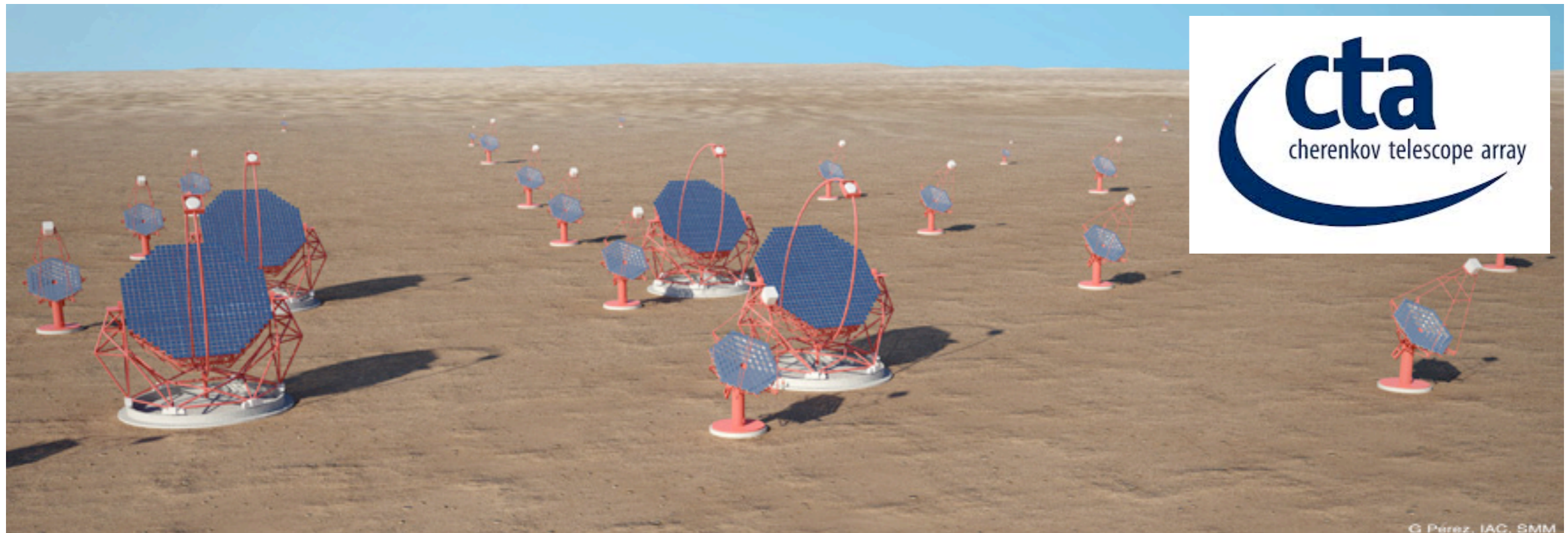
(Slide from F. Zandanel)

Gamma-ray current limits

Representative collection of flux upper limits derived for individual clusters
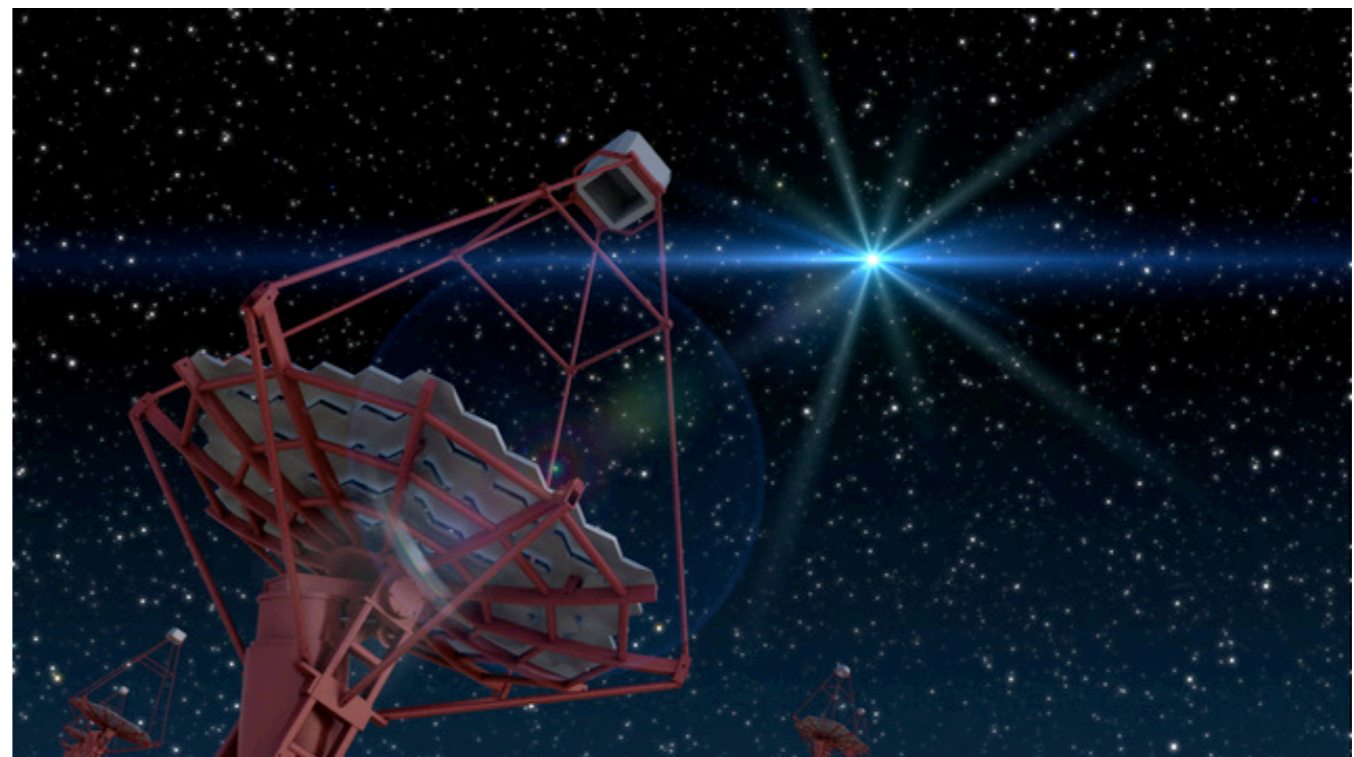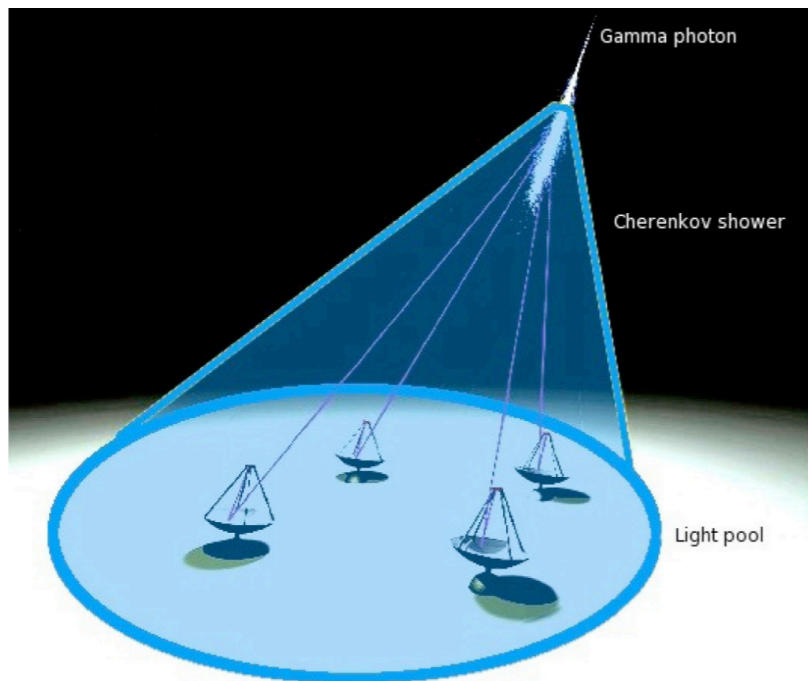
Gamma-ray future: CTA

Questions?